

## Removal of NO<sub>x</sub> and NO<sub>y</sub> in Asian outflow plumes: Aircraft measurements over the western Pacific in January 2002

N. Takegawa,<sup>1</sup> Y. Kondo,<sup>1</sup> M. Koike,<sup>2</sup> G. Chen,<sup>3</sup> T. Machida,<sup>4</sup> T. Watai,<sup>5</sup>  
D. R. Blake,<sup>6</sup> D. G. Streets,<sup>7</sup> J.-H. Woo,<sup>8</sup> G. R. Carmichael,<sup>8</sup> K. Kita,<sup>9</sup>  
Y. Miyazaki,<sup>1</sup> T. Shirai,<sup>10,11</sup> J. B. Liley,<sup>12</sup> and T. Ogawa<sup>10</sup>

Received 5 April 2004; revised 13 July 2004; accepted 30 July 2004; published 19 October 2004.

[1] The Pacific Exploration of Asian Continental Emission Phase A (PEACE-A) aircraft measurement campaign was conducted over the western Pacific in January 2002. Correlations of carbon monoxide (CO) with carbon dioxide (CO<sub>2</sub>) and back trajectories are used to identify plumes strongly affected by Asian continental emissions. ΔCO/ΔCO<sub>2</sub> ratios (i.e., linear regression slopes of CO-CO<sub>2</sub>) in the plumes generally fall within the variability range of the CO/CO<sub>2</sub> emission ratios estimated from an emission inventory for east Asia, demonstrating the consistency between the aircraft measurements and the emission characterization. Removal rates of reactive nitrogen (NO<sub>x</sub> and NO<sub>y</sub>) for the study region (altitude <4 km, 124°–140°E, 25°–45°N) are estimated using the correlation with CO<sub>2</sub>, the photochemical age of the plumes, and the NO<sub>x</sub>/CO<sub>2</sub> emission ratio derived from the emission inventory. The plume age is estimated from the rates of hydrocarbon decay and hydroxyl radical (OH) concentration calculated using a constrained photochemical box model. The average lifetime of NO<sub>x</sub> is estimated to be 1.2 ± 0.4 days. Possible processes controlling the NO<sub>x</sub> lifetime are discussed in conjunction with results from earlier studies. The average lifetime of NO<sub>y</sub> is estimated to be 1.7 ± 0.5 days, which is comparable to the NO<sub>y</sub> lifetime of 1.7–1.8 days that has been previously reported for outflow from the United States. This similarity suggests the importance of chemical processing near the source regions in determining the NO<sub>y</sub> abundance. *INDEX TERMS:* 0322 Atmospheric Composition and Structure: Constituent sources and sinks; 0365 Atmospheric Composition and Structure: Troposphere—composition and chemistry; 0368 Atmospheric Composition and Structure: Troposphere—constituent transport and chemistry; *KEYWORDS:* reactive nitrogen, removal process, Asian outflow

**Citation:** Takegawa, N., et al. (2004), Removal of NO<sub>x</sub> and NO<sub>y</sub> in Asian outflow plumes: Aircraft measurements over the western Pacific in January 2002, *J. Geophys. Res.*, 109, D23S04, doi:10.1029/2004JD004866.

### 1. Introduction

[2] Fossil fuel combustion and biomass burning in east Asia are large sources of trace gases such as carbon monoxide (CO), carbon dioxide (CO<sub>2</sub>), nitrogen oxides (NO<sub>x</sub>), sulfur dioxide (SO<sub>2</sub>), and volatile organic compounds (VOCs) [Streets *et al.*, 2003]. These emissions can significantly affect the distribution of ozone (O<sub>3</sub>) over the western Pacific, and even the United States by long-range intercontinental transport [Jaffe *et al.*, 2003]. To assess the impact of Asian emissions on O<sub>3</sub> and its precursors on regional/hemispheric scales, it is important to evaluate the loss rate of reactive nitrogen species (NO<sub>x</sub> and NO<sub>y</sub>) during transport processes, because the concentrations of these species often control the rate of photochemical O<sub>3</sub> production.

[3] A number of aircraft/ground-based measurements have been conducted in east Asia to investigate the chemical characteristics of Asian outflow. The NASA Pacific Exploratory Mission-West campaigns (PEM-West A: September–October 1991; PEM-West B: February–March 1994) were the first systematic studies focusing on the impact of Asian

<sup>1</sup>Research Center for Advanced Science and Technology, University of Tokyo, Tokyo, Japan.

<sup>2</sup>Department of Earth and Planetary Science, University of Tokyo, Tokyo, Japan.

<sup>3</sup>NASA Langley Research Center, Hampton, Virginia, USA.

<sup>4</sup>National Institute for Environmental Studies, Ibaraki, Japan.

<sup>5</sup>Global Environmental Forum, Ibaraki, Japan.

<sup>6</sup>Department of Chemistry, University of California, Irvine, California, USA.

<sup>7</sup>Decision and Information Sciences Division, Argonne National Laboratory, Argonne, Illinois, USA.

<sup>8</sup>Center for Global and Regional Environmental Research, University of Iowa, Iowa City, Iowa, USA.

<sup>9</sup>Department of Environmental Science, Ibaraki University, Ibaraki, Japan.

<sup>10</sup>Earth Observation Research and Application Center, Japan Aerospace Exploration Agency, Tokyo, Japan.

<sup>11</sup>Now at National Institute for Environmental Studies, Ibaraki, Japan.

<sup>12</sup>National Institute of Water and Atmospheric Research, Lauder, New Zealand.

outflow over the western Pacific [Hoell *et al.*, 1996, 1997]. The NASA Transport and Chemical Evolution over the Pacific (TRACE-P) mission was conducted in the same region in February–April 2001, deploying improved instrumentation and using three-dimensional chemical transport models (3D-CTMs) [Jacob *et al.*, 2003].

[4] The Pacific Exploration of Asian Continental Emission (PEACE) campaign of the Japan Aerospace Exploration Agency (JAXA) was designed to investigate the chemical characteristics of Asian outflow over the western Pacific in winter and spring. These seasons have not been covered by PEM-West-B and TRACE-P [Kondo *et al.*, 2004b]. The PEACE campaign consists of two phases (phase A: January 2002; phase B: April–May 2002). In this analysis we focus on the data obtained during the PEACE-A campaign. The major purpose of this paper is to estimate the removal rates of NO<sub>x</sub> and NO<sub>y</sub>. A brief description of the aircraft measurements during PEACE-A is given in section 2. An emission inventory for east Asia in January 2002 is described in section 3. We use CO and CO<sub>2</sub> as tracers of Asian outflow, and the method of our analysis is described in section 4. A comparison of the observations with the emission inventory and estimates of the removal rates of NO<sub>x</sub> and NO<sub>y</sub> are presented in section 5.

## 2. Aircraft Measurements

### 2.1. Airborne Instruments

[5] In situ measurements of gases and aerosols were made onboard the Gulfstream-II (G-II) aircraft of the Mitsubishi Diamond Air Service (DAS). Figure 1 shows the flight tracks of the G-II aircraft during the PEACE-A campaign. Thirteen flights were conducted, mainly over the Sea of Japan (35°–45°N) and the East China Sea (20°–35°N) during 6–23 January 2002. The instruments used for the PEACE-A campaign were similar to those used for the Biomass Burning and Lightning Experiment Phase B (BIBLE-B) campaign [Kondo *et al.*, 2002]. A brief description of the key measurements in this analysis is given below. CO mixing ratios were measured using a vacuum ultraviolet (VUV) resonance fluorescence technique with a time resolution of 1 s [Takegawa *et al.*, 2001]. CO<sub>2</sub> was measured using a nondispersive infrared absorption (NDIR) technique with a time resolution of 1 s (LI-COR) [Machida *et al.*, 2002]. Measurements of non-methane hydrocarbons (NMHCs) were made using a whole air sampling technique followed by laboratory analysis [Blake *et al.*, 2003]. The integration time of the whole air sampling was typically 40–60 s at lower altitudes (<4 km). O<sub>3</sub> was measured using a dual-beam UV photometer [Kita *et al.*, 2002].

[6] Nitric oxide (NO) and total reactive nitrogen (NO<sub>y</sub>) were measured using a NO-O<sub>3</sub> chemiluminescence detector with a time resolution of 1 s [Kondo *et al.*, 1997b, 2003, 2004a]. Photostationary NO<sub>2</sub> mixing ratios were calculated using a photochemical box model. The box model used in this analysis is the same as that used by Kondo *et al.* [2004b]. The reactions of NO with O<sub>3</sub> and peroxy radicals (HO<sub>2</sub>, CH<sub>3</sub>O<sub>2</sub>, C<sub>2</sub>H<sub>5</sub>O<sub>2</sub>, ...) were taken into consideration. The peroxy radical concentrations were calculated assuming photochemical steady state. The sum of observed NO and calculated NO<sub>2</sub> is given as NO<sub>x</sub>. The precision and accuracy

of the 1-s NO<sub>x</sub> data were estimated to be 13 pptv and 20%, respectively.

[7] NO<sub>y</sub> compounds were catalytically converted to NO on the surface of a gold tube heated at 300°C. The effect of particulate nitrate (NO<sub>3</sub><sup>-</sup>) on the NO<sub>y</sub> measurements is estimated here. During PEACE-A, two converter systems were placed in the aircraft pod and were connected to two independent inlets: one directed forward and the other rearward. The forward and rearward NO<sub>y</sub> systems used during PEACE-A are similar to those used during the SAGE III Ozone Loss and Validation Experiment (SOLVE) campaign [Kondo *et al.*, 2003; Irie *et al.*, 2004]. NO<sub>y</sub> measurements made using the forward facing inlet are referred to as NO<sub>y</sub>(*f*) and those using the rearward facing inlet as NO<sub>y</sub>(*r*). The particle collection efficiency for the rearward facing inlet during PEACE-A was estimated to be nearly 100% for particle diameters (*D<sub>p</sub>*) < 0.4 μm and almost zero for *D<sub>p</sub>* > 3 μm, on the basis of simple aerodynamic calculations [Hinds, 1998]. Although the conversion efficiency for nitrate aerosols was not fully evaluated in the laboratory, our recent TRACE-P analysis has demonstrated that the NO<sub>y</sub>(*r*) represents the sum of gas-phase NO<sub>y</sub> and submicron nonrefractory NO<sub>3</sub><sup>-</sup> aerosols [Kondo *et al.*, 2004a]. Note that nonrefractory means volatile at the temperature of the NO<sub>y</sub> converter (300°C) (e.g., NH<sub>4</sub>NO<sub>3</sub>). The amount of nonrefractory NO<sub>3</sub><sup>-</sup> on larger particles (>0.4 μm) that are not efficiently detected by the rearward NO<sub>y</sub> system can be estimated using the difference between the forward and rearward NO<sub>y</sub>,

$$\text{Nonrefractory NO}_3^- = [\text{NO}_y(f) - \text{NO}_y(r)]/\text{EF}, \quad (1)$$

where EF (>10 for *D<sub>p</sub>* > 0.4 μm) represents the enhancement factor for the forward facing inlet due to subsokinetic sampling. Strictly speaking, equation (1) gives an upper limit of NO<sub>3</sub><sup>-</sup> on larger particles because NO<sub>y</sub>(*f*) also includes NO<sub>3</sub><sup>-</sup> on smaller particles with an enhancement factor larger than unity. Figure 2 shows the correlation of NO<sub>y</sub>(*f*) and NO<sub>y</sub>(*r*) for the entire data set used in this analysis. Ninety-two percent of the data points lie below the 2:1 correspondence line and >99% of the data points lie below the 5:1 line. Given NO<sub>y</sub>(*f*) < 2NO<sub>y</sub>(*r*) and EF > 10, the ratio of nonrefractory NO<sub>3</sub><sup>-</sup> to NO<sub>y</sub>(*r*) is estimated to be <10%. Therefore the amount of nonrefractory NO<sub>3</sub><sup>-</sup> on larger particles was generally small as compared to NO<sub>y</sub>(*r*) during PEACE-A. Hereafter NO<sub>y</sub>(*r*) is expressed simply as NO<sub>y</sub> and is used for the present analysis. Thus the term “removal of NO<sub>y</sub>” in this analysis represents either dry/wet deposition of NO<sub>y</sub> compounds or conversion of NO<sub>y</sub> compounds to refractory NO<sub>3</sub><sup>-</sup> aerosols (e.g., Ca(NO<sub>3</sub>)<sub>2</sub>, NaNO<sub>3</sub>). Because such conversion is generally an irreversible process, it can be regarded as an ultimate sink of NO<sub>y</sub> in the atmosphere.

### 2.2. Vertical Profiles

[8] Figure 3 shows an example of vertical profiles of CO, CO<sub>2</sub>, NO<sub>x</sub>, NO<sub>y</sub>, O<sub>3</sub>, and relative humidity (RH) observed over the Sea of Japan (135°E, 36°N) on 11 January 2002 (flight 04). Large enhancements of CO mixing ratios (200–400 parts per billion by volume (ppbv)) were observed below 2.5 km. The CO mixing ratios between 2.5 and 4 km were lower (i.e., 100–200 ppbv), and those above 4 km

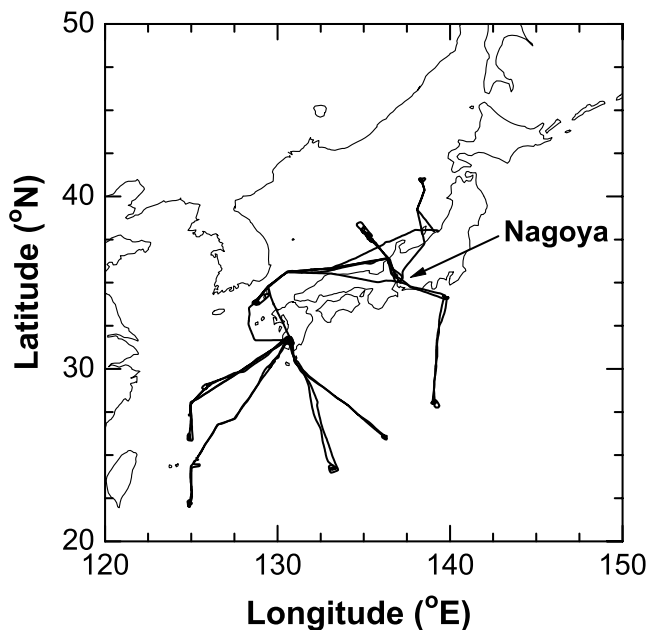


**Figure 1.** Flight tracks of the Gulfstream-II (G-II) aircraft during the Pacific Exploration of Asian Continental Emission Phase A (PEACE-A) campaign.

were fairly constant at  $\sim 100$  ppbv. Correspondingly, the RH profile showed a slight decrease at 2.5 km and a sharp gradient at 4 km. The former is interpreted as the top of the convective boundary layer where the air masses were well mixed, and the latter as the top of the planetary boundary layer where the air masses had been influenced by surface emissions but not well mixed. The CO<sub>2</sub> and NO<sub>y</sub> profiles exhibit almost the same vertical structures as the CO profile. There is no clear structure in the O<sub>3</sub> profile. A detailed analysis of the O<sub>3</sub> production and loss rates during PEACE-A is presented by *Kondo et al.* [2004b].

[9] Profiles similar to Figure 3 were frequently observed during PEACE-A, and we rarely found significant enhancements of primary emissions such as CO, CO<sub>2</sub>, and NO<sub>y</sub> above 4 km. Reanalysis data from the National Centers for Environmental Prediction (NCEP) (<http://www.ncep.noaa.gov/>) indicate that airflow patterns in the boundary layer over east Asia were strongly influenced by the Siberian High in January 2002. It is likely that the vertical transport of trace gases was limited during PEACE-A because of the strong influence of the Siberian High during this period.

### 3. Emission Inventory

#### 3.1. Distribution of CO/CO<sub>2</sub> Emission Ratio

[10] A comprehensive emission inventory of gaseous and particulate emissions in east Asia for the year 2000 has been developed by *Streets et al.* [2003] and evaluated by several investigators using 3-D CTMs [e.g., *Palmer et al.*, 2003; *Woo et al.*, 2003]. *Streets et al.* [2003] showed that the emissions of CO, CO<sub>2</sub>, and other species from the Asian continent tend to have an annual maximum in January mainly because of an increase in domestic heating. An emission inventory for January 2002 was produced for this study taking into account the seasonal trends of gaseous and particulate emissions [*Streets et al.*, 2003] and assuming that

the annually averaged anthropogenic emissions in 2002 were the same as those in 2000. Figure 4 shows a  $1^\circ \times 1^\circ$  grid distribution of CO/CO<sub>2</sub> emission ratios for January 2002. Although the emission inventory includes both anthropogenic and biomass burning sources, major primary emissions such as CO, CO<sub>2</sub>, and NO<sub>x</sub> were likely dominated by anthropogenic sources because the biomass burning activities in east Asia were very weak in January 2002 (e.g., fire images from the Along Track Scanning Radiometer (ATSR) (<http://shark1.esrin.esa.it/ionia/FIRE/AF/ATSR/>)).

[11] Emission ratios for CO/CO<sub>2</sub> have been used as a good proxy for evaluating the combustion efficiency of emission sources, especially for biomass burning studies [e.g., *Yokelson et al.*, 2003]. Lower CO/CO<sub>2</sub> emission ratios correspond to higher combustion efficiency. Because combustion efficiency strongly depends on fuel type (petroleum, coal, etc.) and devices (engine, furnace, etc.), CO/CO<sub>2</sub> emission ratios can be used for diagnosing the types of emission sources. For example, low CO/CO<sub>2</sub> emission ratios ( $<20$  ppbv/ppmv) typically originate from combustion of well-processed gas/liquid fuels (vehicular engines, natural gas stoves, etc.) [e.g., *Zhang et al.*, 2000]. By contrast, high CO/CO<sub>2</sub> emission ratios (30–100 ppbv/ppmv) typically come from combustion of poorly processed solid fuels (coal/biofuel stoves, biomass burning, etc.) [e.g., *Yokelson et al.*, 2003; *Zhang et al.*, 2000]. Fossil fuel power plants, ship engines, and aircraft engines generally have extremely high combustion efficiencies, producing much less CO relative to CO<sub>2</sub> as compared to other sources [e.g., *Nicks et al.*, 2003]. Figure 4 clearly illustrates that the emissions

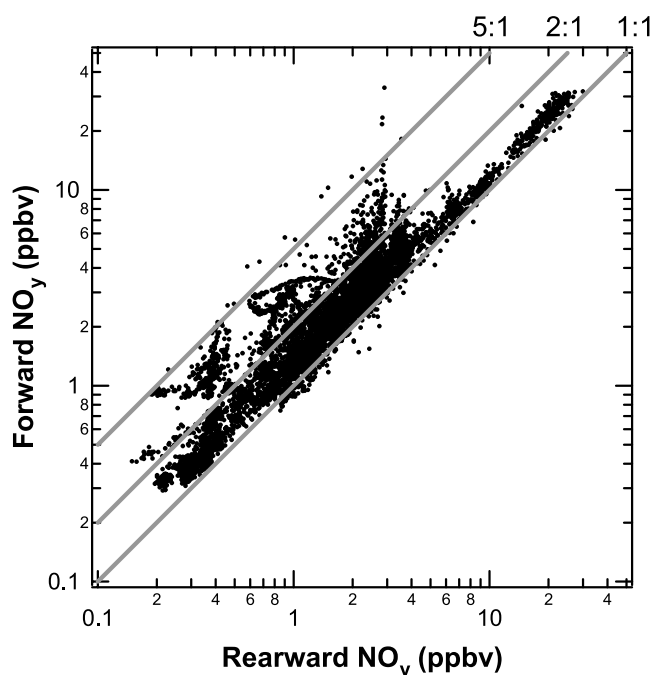


**Figure 2.** Correlation of NO<sub>y</sub> mixing ratios measured using the forward facing inlet (forward NO<sub>y</sub>) and those using the rearward facing inlet (rearward NO<sub>y</sub>). The data points are 1-s averages and represent the entire data set used in this analysis. Shaded lines indicate 1:1, 2:1, and 5:1 correspondence lines.

## Sea of Japan (135°E, 36°N), January 11, 2002

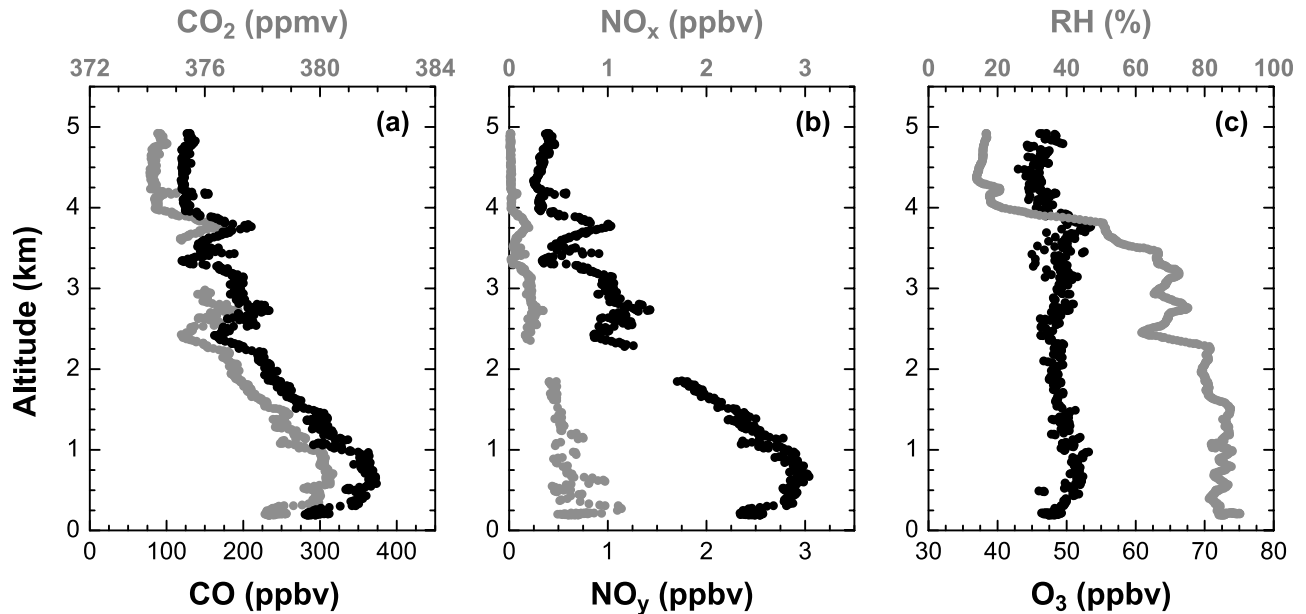


**Figure 3.** Vertical profiles of (a) CO (solid) and CO<sub>2</sub> (shaded); (b) NO<sub>y</sub> (solid) and NO<sub>x</sub> (shaded); and (c) O<sub>3</sub> (solid) and relative humidity (RH) (shaded) observed over the Sea of Japan (135°E, 36°N) on 11 January 2002 (flight 04).

from Japan and South Korea are dominated by high-combustion-efficiency sources, while those from China are dominated by relatively low-combustion-efficiency sources.

### 3.2. Definition of Source Regions

[12] We have classified the source regions into four categories as follows: Japan (mainly Nagoya) (136°–138°E, 34°–36°N), Korea (mainly Pusan) (126°–130°E, 34°–36°N), Northern China (110°–125°E, 35°–44°N), and Central China (105°–123°E, 26°–35°N) (Figure 4). The emission ratios of  $Y$  to  $X$  ( $X, Y = \text{CO}, \text{CO}_2, \text{NO}_x$ , etc.) for the individual source regions were calculated as follows and are summarized in Table 1.

$$E_{Y-X} = \frac{\sum_i F_Y^i}{\sum_i F_X^i} \quad (i = 0, 1, \dots), \quad (2)$$

$$E_{Y-X}^{\text{Max}} = \text{Maximum value of } F_Y^i/F_X^i, \quad (3)$$

$$E_{Y-X}^{\text{Min}} = \text{Minimum value of } F_Y^i/F_X^i. \quad (4)$$

$E_{Y-X}$ ,  $E_{Y-X}^{\text{Max}}$ ,  $E_{Y-X}^{\text{Min}}$  are the average, maximum, and minimum values of the  $Y$  to  $X$  emission ratio, respectively.  $F_X^i$  and  $F_Y^i$  are the emission rates ( $\text{mol month}^{-1} \text{ grid}^{-1}$ ) of species  $X$  and  $Y$  for the  $i$ th grid box in the individual source region, respectively. Only data with  $F_{\text{CO}}^i > 0.2 \text{ Gmol month}^{-1} \text{ grid}^{-1}$  were used to determine the values of  $E_{Y-X}^{\text{Max}}$  and  $E_{Y-X}^{\text{Min}}$  because the variations of  $F_Y^i/F_X^i$  for small emission sources may not be representative. It should be noted that the uncertainties in the emission rates are not taken into

account in determining the maximum and minimum values. The uncertainties in the emission rates are as follows: CO (156% for China, 34% for Japan, and 84% for other east Asia), CO<sub>2</sub> (16% for China, 7% for Japan, and 13% for other east Asia), NO<sub>x</sub> (23% for China, 19% for Japan, and 24% for other east Asia) [Streets *et al.*, 2003].

[13] As described in section 3.1, emissions from Japan (Nagoya) and Korea (Pusan) are dominated by high-combustion-efficiency sources (low CO/CO<sub>2</sub>), while those from Northern/Central China are dominated by low-combustion-efficiency sources (high CO/CO<sub>2</sub>). Details about the interpretation of NO<sub>x</sub>/CO and NO<sub>x</sub>/CO<sub>2</sub> emission ratios are given in section 5.1.2. Note that the ethene (C<sub>2</sub>H<sub>4</sub>) to ethyne (C<sub>2</sub>H<sub>2</sub>) emission ratios are specifically listed in Table 1 because these species are used to estimate the photochemical age of air masses (section 5.2).

## 4. Method of Analysis

### 4.1. Definition of Plumes

[14] The major purpose of this paper is to estimate the removal rates of NO<sub>x</sub> and NO<sub>y</sub> in Asian outflow during PEACE-A. To achieve this goal, we first need to identify air masses that were strongly affected by Asian continental emissions. The  $Y$  to  $X$  enhancement ratio relative to regional background air ( $\Delta Y/\Delta X$  ratio), defined by the linear regression slope of the  $Y$ - $X$  correlation, is used for the air mass identification. The uncertainty in the slope is determined using 68% confidence interval. The regional background air represents relatively clean air that dilutes polluted air masses emitted from anthropogenic sources. Ten-day back trajectories were calculated for the sampled air masses using meteorological data with a horizontal resolution of 1° in longitude and 1° in latitude. The data were provided by the

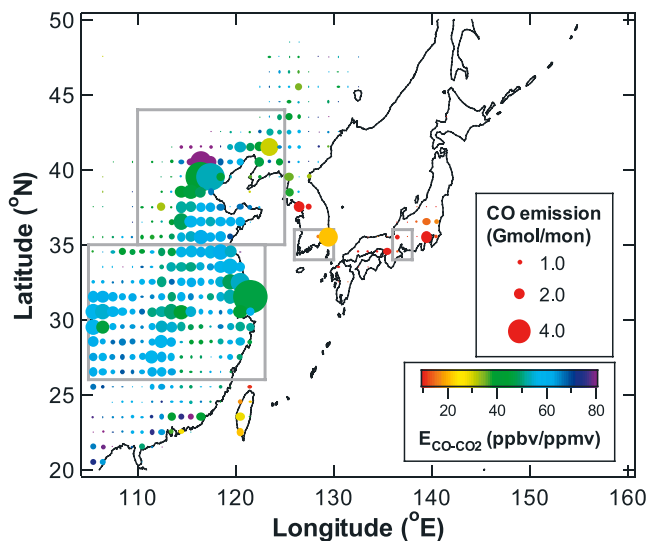


**Figure 4.** The  $1^\circ \times 1^\circ$  grid distribution of CO/CO<sub>2</sub> emission ratios (ppbv/ppmv) for January 2002. The color code represents the CO/CO<sub>2</sub> emission ratios, and the size of the symbols represents the CO emission rate (Gmol month<sup>-1</sup> grid<sup>-1</sup>). Rectangular sections represent the source regions defined in Table 1.

European Centre for Medium-Range Weather Forecasts (ECMWF) (<http://www.ecmwf.int>). In this analysis, “plume” is defined as air masses that meet the following three criteria (criteria 1–3). (1) The air masses were sampled below 4 km, and the back trajectories for the air masses had passed over one of the source regions defined in section 3.2. (2) The enhancement of CO ( $\Delta$ CO) in the air masses is larger than 50 ppbv, and that of CO<sub>2</sub> ( $\Delta$ CO<sub>2</sub>) is larger than 5 parts per million by volume (ppmv). (3) The square of the linear correlation coefficient ( $r^2$ ) for the CO–CO<sub>2</sub> correlation is larger than 0.7.

[15] The threshold values ( $\Delta$ CO > 50 ppbv,  $\Delta$ CO<sub>2</sub> > 5 ppmv,  $r^2 > 0.7$ ) were determined as follows. We assume that air masses observed at 5–7 km (i.e., just above the boundary layer) represent the regional background air. The median mixing ratio ( $\pm$  central 68% range) at 5–7 km was 111 (+15/–15) ppbv for CO and 373 (+0.5/0.6) ppmv for CO<sub>2</sub>. In the case of CO, the threshold value of 50 ppbv was determined so that  $\Delta$ CO values in the plumes are more than 3 times larger than the variability in the regional background air (i.e., 15 ppbv). For CO<sub>2</sub>, the threshold value of 5 ppmv was determined so that  $\Delta$ CO<sub>2</sub> values in the plumes are more than 10 times larger than the variability (0.5–0.6 ppmv). The definition of CO<sub>2</sub> threshold is more conservative than that for CO because vertical gradients of CO<sub>2</sub>

in the boundary layer may be larger than 0.5–0.6 ppmv because of biogenic sources/sinks at the surface. For example, relatively steep gradients of CO<sub>2</sub> (1–2 ppmv between 0 and 3 km) were observed over remote extratropical ocean in the western Pacific region [Machida *et al.*, 2002; Vay *et al.*, 2003]. Using criteria 1 and 2, a total of 21 plumes were identified. The  $r^2$  values were greater than 0.7 for most of the plumes (18 plumes), while the  $r^2$  values were less than 0.6 for the other three plumes. The threshold value of  $r^2 = 0.7$  was determined so as to exclude those statistically less significant plumes.

[16] The identified plumes are summarized in Table 2. The plume ID consists of a group name (e.g., Japan-1, Korea-1, N-China-1, and C-China-1), a flight number (F01, F02, etc.), and a leg number (L01, L02, etc.). First, the duration of each flight was divided into 5–14 flight legs on the basis of sampling altitudes and back trajectories. Second, the source region for each leg was investigated using the trajectories, and the group name was determined corresponding to Table 1. Note that different flight numbers and legs with similar sampling locations on the same day belong to the same group (e.g., both F02L08 and F02L12 belong to Korea-1) but are treated as different plumes. A comparison of the observed  $\Delta$ CO/ $\Delta$ CO<sub>2</sub> ratios to the CO/CO<sub>2</sub> emission ratios estimated from the emission inventory is discussed in section 5.1.1.

[17] The majority of the plumes were sampled below 3 km because the vertical transport was weak during PEACE-A (section 2.2). The infrequent vertical mixing of air masses during the PEACE-A period should have caused the accumulation of pollutants at lower altitudes, leading to the formation of distinct plumes. Indeed, we rarely found such distinct plumes in the same altitude regime during the PEACE-B period (April–May 2002), when the upward lifting by convection was very active over central China [Oshima *et al.*, 2004]. Therefore the plume analysis presented in this study is not applicable to PEACE-B. The differences in photochemical and transport processes between PEACE-A and PEACE-B conditions are discussed by Kondo *et al.* [2004b].

## 4.2. Interpretation of $\Delta Y/\Delta X$ Ratio

[18] Trajectory analysis shows that the transport time from source regions to sampling points was generally less than 4 days. Therefore chemical species with photochemical lifetimes longer than 1 month can be regarded as long-lived, and those with photochemical lifetimes shorter than  $\sim$ 4 days as short-lived. Table 3 summarizes the photochemical lifetimes of CO and NMHCs against reactions with hydroxyl radical (OH) under the conditions experienced during PEACE-A. The diurnally averaged OH concentrations were calculated using a constrained photochemical box model.

**Table 1.** Emission Ratios of Trace Gases for Individual Source Regions<sup>a</sup>

Source Region	Longitude, Latitude	CO/CO <sub>2</sub> , ppbv/ppmv	NO <sub>x</sub> /CO, ppbv/ppbv	NO <sub>x</sub> /CO <sub>2</sub> , ppbv/ppmv	C <sub>2</sub> H <sub>4</sub> /C <sub>2</sub> H <sub>2</sub> , pptv/pptv
Japan (Nagoya)	136°–138°E, 34°–36°N	9 (7–14)	0.21 (0.18–0.23)	1.8 (1.5–2.5)	2.0 (1.9–2.3)
Korea (Pusan)	126°–130°E, 34°–36°N	19 (16–22)	0.22 (0.20–0.23)	4.1 (3.8–4.3)	2.1 (2.0–2.2)
Northern China	110°–125°E, 35°–44°N	52 (30–104)	0.044 (0.022–0.079)	2.3 (1.2–3.3)	1.7 (1.3–3.2)
Central China	105°–123°E, 26°–35°N	56 (38–96)	0.032 (0.013–0.067)	1.8 (0.9–3.8)	1.7 (1.6–2.4)

<sup>a</sup>Average of emission ratios derived from the emission inventory for January 2002. The values in parentheses represent the minimum and maximum values of the emission ratios.

**Table 2.** Plume Identification

Plume ID <sup>a</sup>			Sampling Location			Number of 1-s Data Points	<i>r</i> <sup>2</sup> for CO-CO <sub>2</sub> Correlation	ΔCO/ΔCO <sub>2</sub> <sup>b</sup> ppbv/ppmv
Group	Flight No.	Leg No.	Longitude, °E	Latitude, °N	Altitude, km			
<i>Japan Plumes</i>								
Japan-1	F02	L02	135.8–136.1	36.3–36.4	0.7–2.5	230	0.89	17 (±0.4)
Japan-2	F02	L14	136.9–137.0	35.0–35.2	0.4–1.0	209	0.99	18 (±0.1)
Japan-3	F03	L02	139.4–139.9	32.5–34.2	0.2–1.8	1708	0.79	16 (±0.2)
Japan-4	F03	L08	137.0–137.2	35.0–35.1	0.8–1.6	311	0.99	14 (±0.1)
<i>Korea Plumes</i>								
Korea-1	F02	L08	129.6–131.1	34.9–35.7	0.2–2.0	1302	0.98	24 (±0.1)
Korea-1	F02	L12	128.7–129.7	33.8–34.9	0.2–1.4	1137	0.88	22 (±0.2)
<i>Northern China Plumes</i>								
N-China-1	F04	L02	133.3–136.0	35.9–36.3	0.2–3.9	1867	0.97	38 (±0.2)
N-China-1	F04	L04	132.0–134.9	35.7–36.6	0.2–3.0	1917	0.98	36 (±0.1)
N-China-2	F04	L06	136.2–136.6	37.3–37.4	1.0–3.0	240	0.99	35 (±0.3)
N-China-2	F05	L05	138.1–138.4	39.2–40.2	1.8–4.0	687	0.79	28 (±0.5)
N-China-3	F06	L01	136.9–137.0	35.3–35.4	1.0–2.9	65	0.95	35 (±1)
N-China-3	F06	L03	135.8–136.2	36.3–36.4	1.6–4.0	255	0.98	40 (±0.4)
<i>Central China Plumes</i>								
C-China-1	F07	L02	128.3–128.4	30.1–30.1	1.3–2.0	66	0.99	48 (±0.3)
C-China-1	F07	L09	127.6–128.0	29.8–30.0	1.3–4.0	282	0.96	43 (±0.5)
C-China-2	F07	L05	124.9–125.0	27.5–27.9	1.2–4.0	270	0.94	28 (±0.5)
C-China-2	F07	L07	125.9–126.1	29.0–29.2	1.2–4.0	280	0.77	29 (±1)
C-China-3	F07	L10	130.0–130.8	31.3–31.6	1.3–4.0	910	0.88	36 (±0.4)
C-China-4	F12	L05	130.6–130.9	31.3–31.8	2.0–3.0	1069	0.99	42 (±0.1)

<sup>a</sup>Each plume ID consists of a group name, flight number, and leg number. The durations of individual flights (F01, F02, etc.) were divided into 5–14 flight legs (L01, L02, etc.) on the basis of back trajectories. The name of each group represents the source region (defined in Table 1) estimated from the trajectories. Different flight legs with similar sampling locations on the same day were categorized as the same group.

<sup>b</sup>ΔCO/ΔCO<sub>2</sub> ratios were determined from linear regression analysis.

The data obtained below 3 km were used to calculate the median OH concentration because the majority of the plumes were transported below 3 km prior to the measurements. The median value (± central 68% range) of OH concentration was  $5 (+6/-3) \times 10^5 \text{ cm}^{-3}$ . The kinetic parameters listed by *Atkinson et al.* [1992] and *Calvert et al.* [2000] were used for calculating the rates of OH reactions. In Table 3, CO, ethane (C<sub>2</sub>H<sub>6</sub>), and C<sub>2</sub>H<sub>2</sub> correspond to long-lived species, and C<sub>2</sub>H<sub>4</sub> and propene (C<sub>3</sub>H<sub>6</sub>) correspond to short-lived species.

[19] If *X* and *Y* are both long-lived, the Δ*Y*/Δ*X* ratio should be equal to the *E*<sub>*Y-X*</sub> (or between *E*<sub>*Y-X*</sub><sup>Max</sup> and *E*<sub>*Y-X*</sub><sup>Min</sup>) of the source region estimated from the trajectories. If *X* is a long-lived species and *Y* is a short-lived species, the Δ*Y*/Δ*X* ratio should be systematically smaller than *E*<sub>*Y-X*</sub> because of the removal (including both photochemical loss and deposition) of species *Y*. In this case, we assume that the Δ*Y*/Δ*X* ratio is approximated as

$$\Delta Y/\Delta X = E_{Y-X} \exp(-t/\tau_Y) \cdot (X : \text{long-lived}; Y : \text{short-lived}), \quad (5)$$

where *t* and τ<sub>*Y*</sub> are the elapsed time since emission and the removal lifetime of species *Y*, respectively.

[20] Strictly speaking, Δ*Y*/Δ*X* ratios are affected by chemical and dilution processes, and these two effects are generally not distinguishable [*Parrish et al.*, 1992; *McKeen et al.*, 1996; *Takegawa et al.*, 2003]. However, we can use the equation (5) under the conditions where the mixing ratio of *Y* in the background air is much smaller than that in the plume. This condition is applicable to the short-lived

species considered in this analysis (i.e., *Y* = NO<sub>x</sub>, NO<sub>y</sub>, C<sub>2</sub>H<sub>4</sub>).

## 5. Results and Discussion

### 5.1. Comparison of Observations With Emission Inventory

#### 5.1.1. CO/CO<sub>2</sub> Emission Ratio

[21] The ΔCO/ΔCO<sub>2</sub> ratios observed in the plumes can be directly compared to the CO/CO<sub>2</sub> emission ratios from the source regions because the production and loss of CO during transport should be negligible on a timescale of ~4 days. We consider that biogenic sources/sinks of CO<sub>2</sub> such as vegetation did not significantly affect the ΔCO/ΔCO<sub>2</sub> ratios for this analysis because of the following two reasons. First, gross flux of CO<sub>2</sub> from/to vegetation is likely small during the PEACE-A period because biogenic activity is weak in winter. Second, we have chosen distinct plumes in which the enhancements of CO<sub>2</sub> are large (>5 ppmv) and the correlation of CO versus CO<sub>2</sub> is tight (*r*<sup>2</sup> > 0.7).

**Table 3.** Photochemical Lifetime of CO and NMHCs Under the Conditions Experienced During PEACE-A

Species	Lifetime, <sup>a</sup> days
CO	100
Ethane (C <sub>2</sub> H <sub>6</sub> )	120
Ethene (C <sub>2</sub> H <sub>4</sub> )	2.7
Ethyne (C <sub>2</sub> H <sub>2</sub> )	35
Propane (C <sub>3</sub> H <sub>8</sub> )	24
Propene (C <sub>3</sub> H <sub>6</sub> )	0.8

<sup>a</sup>Median value of the diurnally averaged OH concentration of  $5 \times 10^5 \text{ cm}^{-3}$  (<3 km, 25°–45°N) was used for the calculation.

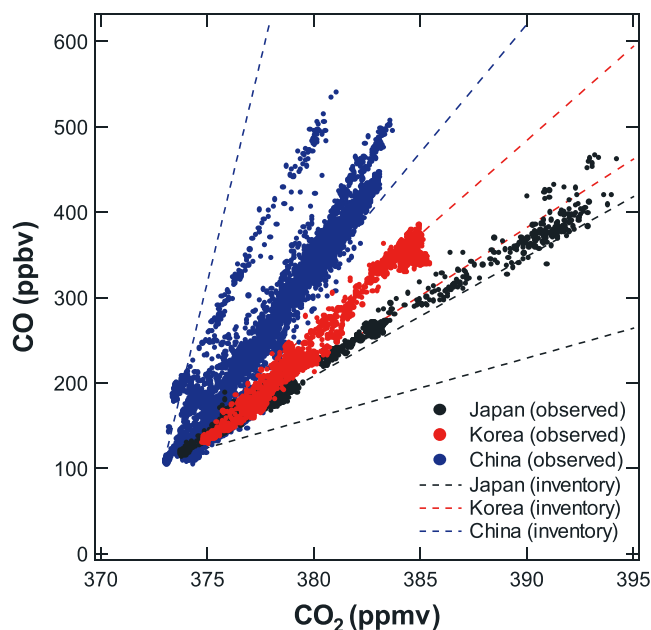


**Figure 5.** Correlation of CO with CO<sub>2</sub> for the plumes listed in Table 2. The data are 1-s averages. Black, red, and blue dots represent the Japan, Korea, and China plumes, respectively (Table 2). The China plumes include both Northern and Central China plumes. The dashed lines represent the variability range of the CO/CO<sub>2</sub> emission ratios in the individual source regions estimated from the emission inventory.

Vegetation is generally distributed over a wide area as compared to the anthropogenic sources. Thus it should affect the CO<sub>2</sub> mixing ratios in regional background air (i.e., air masses that dilute the plumes) rather than in the formation of such distinct plumes.

[22] Figure 5 shows correlations of CO versus CO<sub>2</sub> for all of the plumes listed in Table 2. The most important feature is that the observed  $\Delta\text{CO}/\Delta\text{CO}_2$  ratios exhibit distinct values depending on the source region, indicating that they can be used as a good tracer for investigating the origins of anthropogenic plumes. In addition, the observed  $\Delta\text{CO}/\Delta\text{CO}_2$  ratio falls within the variability range of the CO/CO<sub>2</sub> emission ratio for most of the plumes, demonstrating the overall consistency among the aircraft measurements, trajectories, and emission characterization. We note that the observed  $\Delta\text{CO}/\Delta\text{CO}_2$  ratios were higher by a factor of 1.5–2 than the average CO/CO<sub>2</sub> emission ratio for the Japan plumes (Table 2). Considering that the uncertainty in the emission rate of CO is much larger than that of CO<sub>2</sub> for Japan (and also for the other regions), it is suggested that the discrepancy is mainly due to the uncertainty in the CO emission rate in the emission inventory. However, difference between observed  $\Delta\text{CO}/\Delta\text{CO}_2$  ratios and emission inventory does not significantly affect the identification of plumes as long as it is smaller than or comparable to the variability range of the CO/CO<sub>2</sub> emission ratio in the emission inventory.

[23] Examples of individual plumes are shown in Figures 6 and 7 (Korea-1 (F02L08) and N-China-1 (F04L02) plumes in Table 2, respectively). These figures include the sampling points color-coded by CO mixing ratio,

back trajectory, and CO–CO<sub>2</sub> correlation for the plumes. The  $\Delta\text{CO}/\Delta\text{CO}_2$  ratio observed in the Korea-1 (F02L08) plume was higher by  $\sim 25\%$  than the average CO/CO<sub>2</sub> emission ratio from the Korea region. On the other hand, the  $\Delta\text{CO}/\Delta\text{CO}_2$  ratio observed in the N-China-1 (F04L02) plume was lower by  $\sim 30\%$  than the average CO/CO<sub>2</sub> emission ratio from the Northern China region. A similar tendency is found for the other plumes (Table 2). However, these small discrepancies may not be significant when we take into account the variability range (i.e., minimum and maximum values) of the CO/CO<sub>2</sub> emission ratios.

[24] Correlations of halocarbons with CO can provide additional information on the chemical characteristics of the plumes. Figures 8 and 9 depict the correlations of methyl bromide (CH<sub>3</sub>Br) and Halon-1211 (H-1211) with CO in the Korea-1 (F02L08) and N-China-1 (F04L02) plumes, respectively (same plumes as Figures 6 and 7). *Blake et al.* [2003] found that CH<sub>3</sub>Br is a good tracer of Japan and Korea emissions and H-1211 is a good tracer of China emissions, on the basis of the whole air samples collected during the TRACE-P campaign. The Korea plume shows a higher  $\Delta\text{CH}_3\text{Br}/\Delta\text{CO}$  ratio and lower  $\Delta(\text{H-1211})/\Delta\text{CO}$  ratio than the Northern China plume, which is consistent with the findings of *Blake et al.* [2003]. Although the CH<sub>3</sub>Br–CO correlation in the Korea plume exhibits a large scatter ( $r^2 = 0.39$ ), the systematic difference between these two plumes supports the validity of plume identification applied in this study.

#### 5.1.2. NO<sub>x</sub>/CO and NO<sub>x</sub>/CO<sub>2</sub> Emission Ratios

[25] Two fresh plumes were sampled below 1.5 km over Nagoya, Japan on 7 and 10 January 2002 (Japan-2 (F02L14) and Japan-4 (F03L08) plumes in Table 2). Figures 10a and 10b show the correlations of NO<sub>y</sub> with CO and CO<sub>2</sub> in the plumes. Assuming that loss of NO<sub>y</sub> in these fresh plumes was negligible, the  $\Delta\text{NO}_y/\Delta\text{CO}$  (or  $\Delta\text{NO}_y/\Delta\text{CO}_2$ ) ratios for these plumes can be interpreted as the NO<sub>x</sub>/CO (or NO<sub>x</sub>/CO<sub>2</sub>) emission ratios for this region. The observed  $\Delta\text{NO}_y/\Delta\text{CO}$  ratios were lower by a factor of  $\sim 2$  than the average NO<sub>x</sub>/CO emission ratio estimated from the emission inventory (Figure 10a). By contrast, the observed  $\Delta\text{NO}_y/\Delta\text{CO}_2$  ratios showed good agreement with the emission inventory (Figure 10b). As discussed in section 5.1.1, we suggest that the discrepancy in the NO<sub>x</sub>/CO emission ratio is mainly due to the uncertainty in the CO emission rate. The uncertainty in the NO<sub>x</sub>/CO emission ratio in the emission inventory has a significant influence on the estimates of removal rates of NO<sub>x</sub> and NO<sub>y</sub>, if we use CO as a tracer of NO<sub>x</sub> and NO<sub>y</sub>.

[26] To obtain a better understanding of NO<sub>x</sub>/CO<sub>2</sub> emission ratios from various sources, we show data observed in fresh savanna fire plumes over northern Australia during the BIBLE-B campaign for comparison [*Shirai et al.*, 2003; *Takegawa et al.*, 2003]. The  $\Delta\text{CO}/\Delta\text{CO}_2$ ,  $\Delta\text{NO}_y/\Delta\text{CO}$ , and  $\Delta\text{NO}_y/\Delta\text{CO}_2$  ratios observed in fresh savanna fire plumes were 86 ppbv/ppmv, 0.018 ppbv/ppbv, and 1.5 ppbv/ppmv, respectively. There is a significant difference in the  $\Delta\text{NO}_y/\Delta\text{CO}$  ratios between Nagoya (PEACE-A) and Australia (BIBLE-B), while the  $\Delta\text{NO}_y/\Delta\text{CO}_2$  ratios are comparable. It has been pointed out that the NO<sub>x</sub>/CO<sub>2</sub> emission ratios from biomass burning are relatively uniform ( $2 \pm 1$  ppbv/ppmv) for various types of fires, although they have a dependence on the nitrogen content of the fuels [*Andreae*

## Korea-1 (F02L08) plume - January 7, 2002

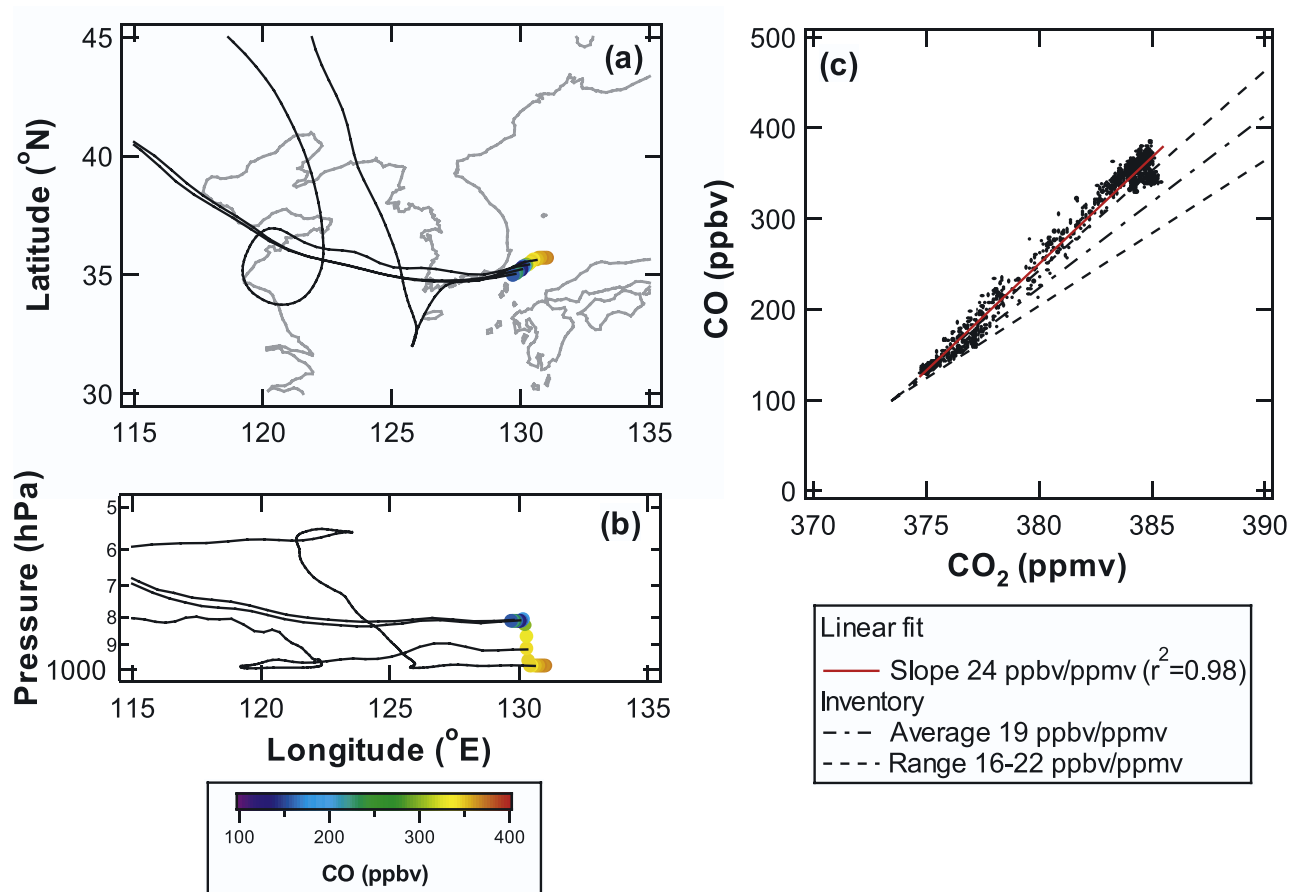


**Figure 6.** (a and b) Air masses observed off Korea on 7 January 2002. The data points are 60-s averages and color-coded by CO mixing ratios. These air masses correspond to the Korea-1 (F02L08) plume in Table 2. Back trajectories for the plume are indicated by solid lines. (c) Correlation of CO and CO<sub>2</sub> in the plume (solid circles). The data are 1-s averages. The red line represents the linear regression for the data. The dot-dashed line and two dashed lines represent the average, maximum, and minimum values of the CO/CO<sub>2</sub> emission ratio from the Korea region, respectively.

*et al.*, 1994; Yokelson *et al.*, 2003; and references therein]. The results obtained in this study suggest that the uniformity of NO<sub>x</sub>/CO<sub>2</sub> emission ratios holds even though the types of emission sources are significantly different from biomass burning.

[27] The preceding discussion provides some insights into the merits and disadvantages of using CO or CO<sub>2</sub> as a tracer of NO<sub>x</sub> from combustion sources. CO<sub>2</sub> is a good tracer for NO<sub>x</sub> because these two species are major products of high-combustion-efficiency processes, while biogenic interactions of CO<sub>2</sub> sometimes make it difficult to define the signals from combustion sources, especially for aged air masses. CO does not have interactions with biogenic sources/sinks, while NO<sub>x</sub>/CO emission ratios show a large variability depending on the combustion efficiency, especially for the cases where the emission sources are heterogeneous. In addition, the uncertainty in the emission rate of CO is generally much larger than that of CO<sub>2</sub>. In the present analysis we have chosen only distinct plumes where the enhancements of CO<sub>2</sub> are large (>5 ppmv) and the correlation of CO versus CO<sub>2</sub> is tight ( $r^2 > 0.7$ ). Therefore we

choose CO<sub>2</sub> as a tracer of NO<sub>x</sub> rather than CO to estimate the removal rates of NO<sub>x</sub> and NO<sub>y</sub>.

### 5.2. Plume Age Derived From Hydrocarbons

[28] The elapsed time since emission for each plume (plume age) can be estimated using equation (5) and a pair of NMHCs with known photochemical lifetimes (Table 3). We define plume age ( $t$ ) as follows:

$$t = \overline{\tau_{C_2H_4}} [\ln(E_{C_2H_4-C_2H_2}) - \ln(\Delta C_2H_4/\Delta C_2H_2)], \quad (6)$$

where  $\overline{\tau_{C_2H_4}}$  (=2.7 days) is the average lifetime of C<sub>2</sub>H<sub>4</sub> during PEACE-A (Table 3). We have chosen C<sub>2</sub>H<sub>2</sub> as a long-lived species and C<sub>2</sub>H<sub>4</sub> as a short-lived species because of the following two reasons. First, the lifetime of C<sub>2</sub>H<sub>4</sub> is 2.7 days, so that the photochemical history of the plumes (typically <4 days old) can be clearly resolved. Second, the emission ratio of C<sub>2</sub>H<sub>4</sub> to C<sub>2</sub>H<sub>2</sub> ( $E_{C_2H_4-C_2H_2}$ ) does not significantly depend on the region of emission (Table 1). The uniformity of the C<sub>2</sub>H<sub>4</sub>/C<sub>2</sub>H<sub>2</sub> emission ratio is understandable considering the similarity in the emission

## N-China-1 (F04L02) plume - January 11, 2002

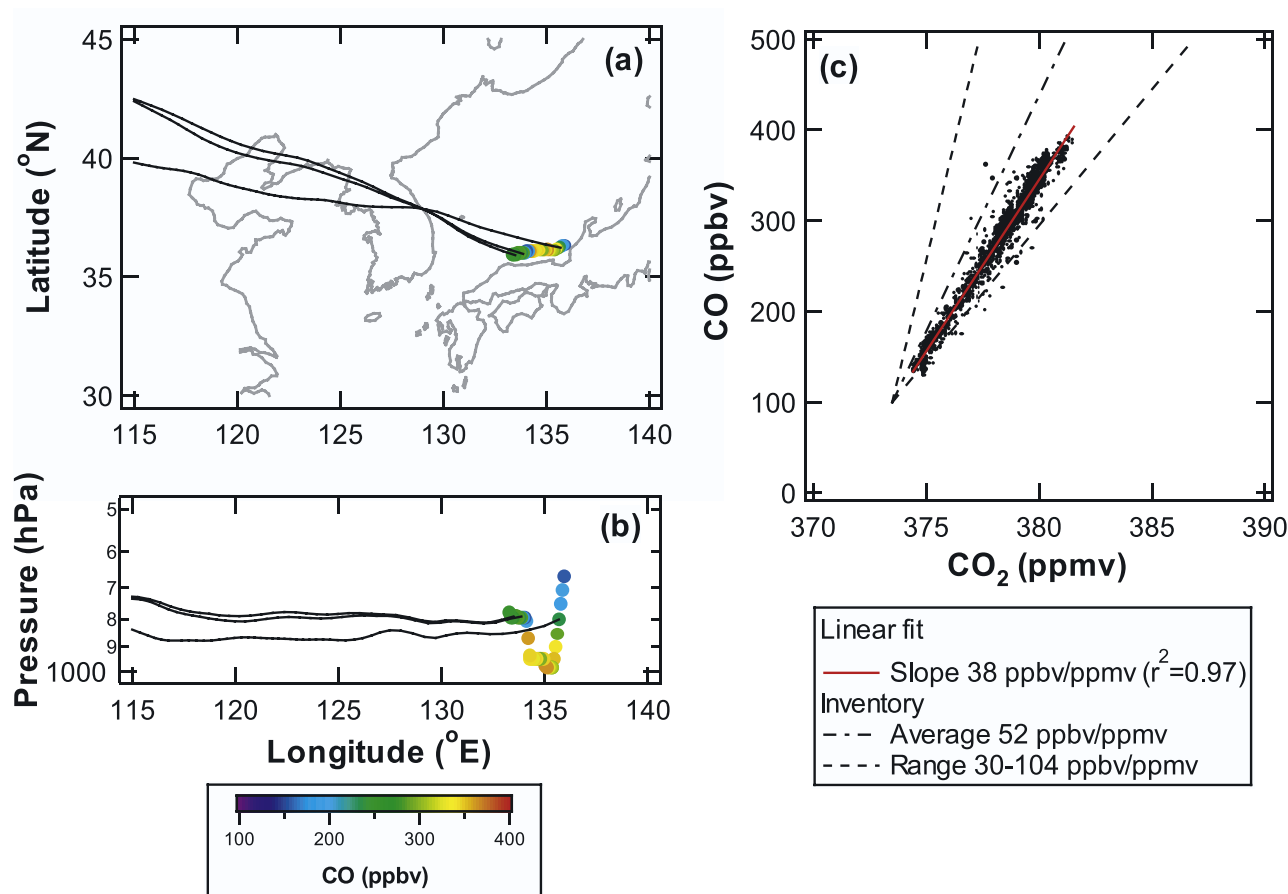


**Figure 7.** Same plot as Figure 6 but for air masses transported from northern China observed on 11 January 2002. These air masses correspond to the N-China-1 (F04L02) plume in Table 2.

patterns of these two species, which are dominated by biofuel burning and transportation for east Asia [Streets *et al.*, 2003, Figure 6].

[29] The plume age estimated for each plume is shown in Table 4. The number of plumes is smaller than that in Table 2 because it is limited by the availability of NMHC data. The uncertainty in the plume age was estimated from the fitting error in determining the  $\Delta C_2H_4/\Delta C_2H_2$  ratio and the maximum and minimum values of the emission ratio given by equations (3) and (4). The variability range of the OH concentration (see section 4.2) is not included in the error estimate. In addition, injection of fresh emissions of hydrocarbons into the plumes during transport is another source of uncertainty [Parrish *et al.*, 1992] that is not included in the error estimate.

[30] For comparison, transport time was roughly estimated on the basis of the trajectories and is listed in Table 4. The transport time tends to be shorter than the plume age for each plume. There are two possible explanations for this discrepancy. First, the transport time does not include the residence time (stagnant time) near the source region. Second, the plume age might be overestimated if OH concentrations in the plumes were actually higher than the median value of the model-predicted OH concentration

( $5 \times 10^5 \text{ cm}^{-3}$ ), especially near the source regions. Indeed, earlier studies have shown that OH concentrations in fresh biomass burning or ship plumes were significantly higher than those in background air [Hobbs *et al.*, 2003; Song *et al.*, 2003]. Without detailed information on the OH chemistry in the plumes for this analysis, however, we use the median value of the model-predicted OH concentration to estimate the plume age.

### 5.3. Removal Rates of NO<sub>x</sub> and NO<sub>y</sub>

[31] Figures 11 and 12 depict the correlations of NO<sub>x</sub> and NO<sub>y</sub> with CO<sub>2</sub> in the Korea-1 (F02L08) and N-China-1 (F04L02) plumes, respectively (same plumes as Figures 6 and 7). For both plumes, the  $\Delta NO_x/\Delta CO_2$  and  $\Delta NO_y/\Delta CO_2$  ratios are significantly lower than the NO<sub>x</sub>/CO<sub>2</sub> emission ratios, indicating that removal of NO<sub>x</sub> and NO<sub>y</sub> occurred within the source region or during the transport from it. From equation (5) we obtain

$$(\Delta NO_x/\Delta CO_2)/E_{NO_x-CO_2} = \exp(-t/\tau_{NO_x}), \quad (7)$$

$$(\Delta NO_y/\Delta CO_2)/E_{NO_x-CO_2} = \exp(-t/\tau_{NO_y}). \quad (8)$$

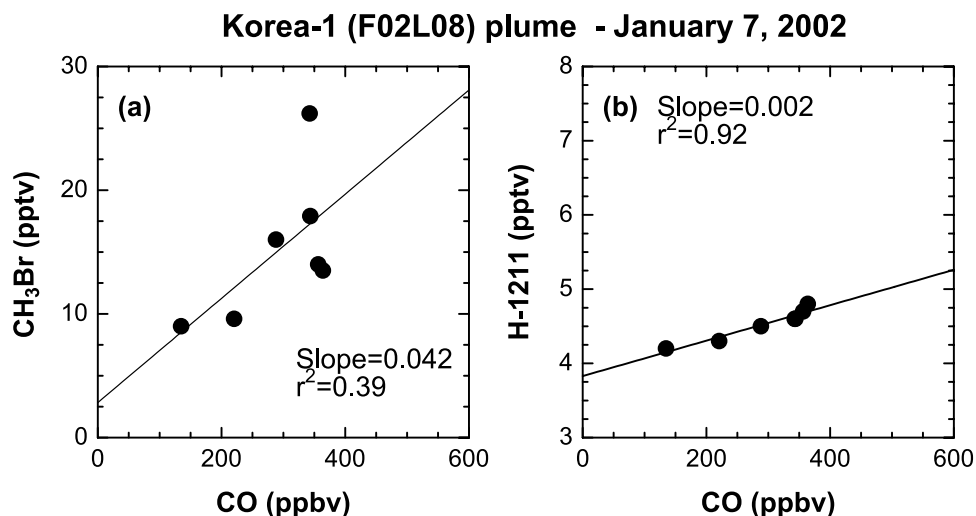


**Figure 8.** Correlations of (a) methyl bromide (CH<sub>3</sub>Br) and (b) Halon-1211 (H-1211) with CO in the Korea-1 (F02L08) plume (same plume as used in Figure 6). Solid lines are linear regression lines. The unit of the slope is pptv/ppbv.

The left-hand sides of these equations give the fractions of NO<sub>x</sub> and NO<sub>y</sub> remaining in the observed plumes. Figures 13a and 13b depict the  $(\Delta\text{NO}_x/\Delta\text{CO}_2)/E_{\text{NO}_x\text{-CO}_2}$  and  $(\Delta\text{NO}_y/\Delta\text{CO}_2)/E_{\text{NO}_x\text{-CO}_2}$  as a function of the plume age ( $t$ ) defined by equation (6), respectively. Each data point corresponds to the linear regression slope for each plume and is colored on the basis of average sampling altitude. The photochemical age is assumed to be zero for the plumes sampled in the boundary layer over Nagoya, Japan because these plumes are considered to be very fresh (section 5.1.2). The uncertainty was estimated from fitting errors for the  $\Delta\text{NO}_x/\Delta\text{CO}_2$  (or  $\Delta\text{NO}_y/\Delta\text{CO}_2$ ) ratio and the maximum and minimum values of the NO<sub>x</sub> to CO<sub>2</sub> emission ratios (Table 1). It is important to note that these plots do not represent a Lagrangian history for a particular event because the plumes were sampled at various locations on various days during PEACE-A. In spite of this variability, there is a

clear tendency that both  $(\Delta\text{NO}_x/\Delta\text{CO}_2)/E_{\text{NO}_x\text{-CO}_2}$  and  $(\Delta\text{NO}_y/\Delta\text{CO}_2)/E_{\text{NO}_x\text{-CO}_2}$  show systematic decrease with plume aging. There is a slight dependence of plume age on altitude. The plumes sampled below 1.2 km (warm colors in Figure 13) have plume ages shorter than 2.5 days, while those sampled above 1.2 km (cold colors) have plume ages longer than 2.5 days. However, there is no significant altitude dependence of the removal rates of NO<sub>x</sub> and NO<sub>y</sub>.

[32] The lifetimes of NO<sub>x</sub> ( $\tau_{\text{NO}_x}$ ) and NO<sub>y</sub> ( $\tau_{\text{NO}_y}$ ) for the individual plumes were estimated using equations (6), (7), and (8) (Table 4). The average lifetimes of NO<sub>x</sub> ( $\overline{\tau_{\text{NO}_x}}$ ) and NO<sub>y</sub> ( $\overline{\tau_{\text{NO}_y}}$ ) were  $1.2 \pm 0.4$  and  $1.7 \pm 0.5$  days, respectively. The errors were determined from the standard deviation (1- $\sigma$ ) of the average, and the uncertainty in the OH concentration (a factor of 2) was not taken into account for the error estimate. An alternative way for estimating  $\overline{\tau_{\text{NO}_x}}$  and  $\overline{\tau_{\text{NO}_y}}$  is to calculate linear regression slopes for the

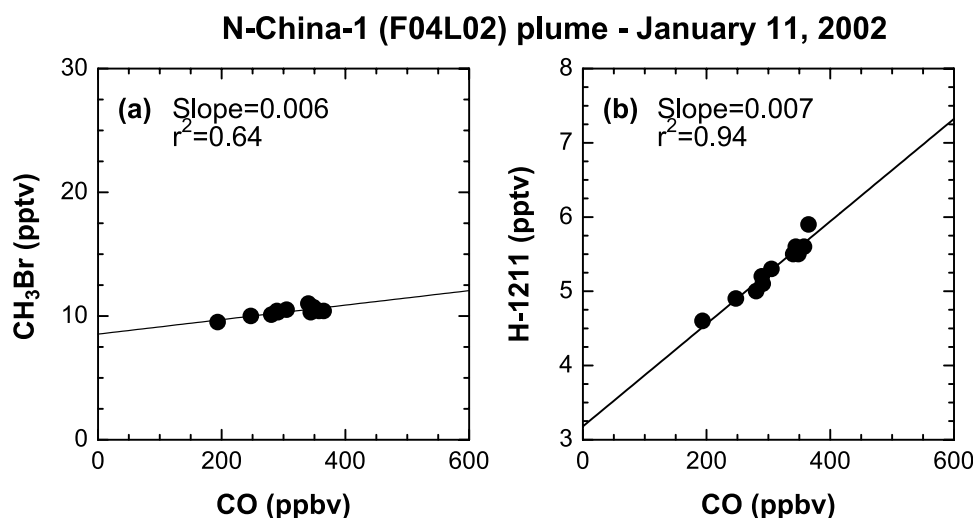


**Figure 9.** Same plot as Figure 8 but for the N-China-1 (F04L02) plume (same plume as used in Figure 7).

**Table 4.** Plume Age and Lifetimes of NO<sub>x</sub> and NO<sub>y</sub> for Individual Plumes

Plume ID		Plume Age, <sup>a</sup> Days	Transport Time, <sup>b</sup> days	NO <sub>x</sub>		NO <sub>y</sub>	
Group	Flight and Leg No.			(ΔNO <sub>x</sub> /ΔCO <sub>2</sub> )/E <sub>NO<sub>x</sub>-CO<sub>2</sub></sub>	τ <sub>NO<sub>x</sub></sub> , days	(ΔNO <sub>y</sub> /ΔCO <sub>2</sub> )/E <sub>NO<sub>x</sub>-CO<sub>2</sub></sub>	τ <sub>NO<sub>y</sub></sub> , days
Japan-1	F02L02	3.0 (+0.3/−0.1)	<1	0.09 (+0.02/−0.03)	1.2 (+0.3/−0.2)	0.19 (+0.04/−0.06)	1.8 (+0.4/−0.4)
Japan-3	F03L02	2.2 (+1.1/−0.8)	<1	0.35 (+0.12/−0.20)	2.1 (+2.3/−1.4)	0.44 (+0.14/−0.24)	2.6 (+3.4/−1.8)
Korea-1	F02L08	1.8 (+0.4/−0.3)	<1	0.15 (+0.01/−0.01)	0.9 (+0.3/−0.2)	0.17 (+0.02/−0.01)	1.0 (+0.3/−0.2)
N-China-1	F04L02	3.1 (+2.0/−0.9)	1–2	0.05 (+0.05/−0.02)	1.0 (+1.1/−0.4)	0.16 (+0.15/−0.05)	1.7 (+2.6/−0.7)
N-China-1	F04L04	2.3 (+1.9/−0.9)	1–2	0.06 (+0.05/−0.02)	0.8 (+1.1/−0.4)	0.17 (+0.16/−0.06)	1.3 (+2.5/−0.6)
C-China-2	F07L05	4.3 (+0.9/−0.3)	1–3	0.02 (+0.02/−0.01)	1.1 (+0.6/−0.2)	0.03 (+0.04/−0.02)	1.3 (+0.8/−0.3)
C-China-2	F07L07	4.0 (+1.0/−0.4)	1–3	0.008 (+0.01/−0.004)	0.8 (+0.4/−0.2)	0.06 (+0.08/−0.03)	1.5 (+1.1/−0.4)
C-China-3	F07L10	3.8 (+0.9/−0.3)	1–3	0.06 (+0.07/−0.03)	1.4 (+1.0/−0.4)	0.14 (+0.17/−0.08)	2.0 (+2.1/−0.7)

<sup>a</sup>Plume age was derived from ΔC<sub>2</sub>H<sub>4</sub>/ΔC<sub>2</sub>H<sub>2</sub> ratios ([OH] = 5 × 10<sup>5</sup> cm<sup>−3</sup>).

<sup>b</sup>Transport time was roughly estimated on the basis of trajectories.

data points of Figures 13a and 13b. They were estimated as  $\overline{\tau_{\text{NO}_x}} = 1.1 \pm 0.3$  days and  $\overline{\tau_{\text{NO}_y}} = 1.6 \pm 0.3$  days, which are close to the values shown above. The errors were determined from 68% confidence intervals for the least squares fit. It should be noted that there is no significant difference in the NO<sub>x</sub> and NO<sub>y</sub> lifetimes between the plumes, suggesting that differences in the emission sources were not an important factor determining the lifetimes of NO<sub>x</sub> and NO<sub>y</sub> during PEACE-A.

[33] The (ΔNO<sub>y</sub>/ΔCO<sub>2</sub>)/E<sub>NO<sub>x</sub>-CO<sub>2</sub></sub> values shown in Table 4 indicate that 80–90% of NO<sub>y</sub> was removed within 4 days following emission. The removal processes should be either dry/wet deposition of NO<sub>y</sub> compounds or conversion of HNO<sub>3</sub> to refractory particles, although quantitative estimates of the contributions from dry and wet deposition are difficult to achieve in this study. Because dry/wet depositions of NO<sub>x</sub> and peroxyacetyl nitrate (PAN) are generally slow, this leads to a hypothesis that the majority (>80–90%) of NO<sub>x</sub> emitted from surface sources was oxidized to HNO<sub>3</sub> or nitrate and a rapid removal of these species occurred in the plumes. PAN could appear as a major form of NO<sub>y</sub> in the plumes, as was observed in Asian outflow during PEM-West B and TRACE-P [Kondo *et al.*, 1997a; Koike *et al.*, 2003], if a majority of HNO<sub>3</sub> and nitrate were removed from the plumes.

[34] To obtain a better understanding of the behavior of NO<sub>x</sub> oxidation products, the average NO<sub>x</sub>/NO<sub>y</sub> ratios and (ΔNO<sub>z</sub>/ΔCO<sub>2</sub>)/E<sub>NO<sub>x</sub>-CO<sub>2</sub></sub> values in the plumes are plotted as a function of plume age (Figures 14a and 14b), where NO<sub>z</sub>(=NO<sub>y</sub>−NO<sub>x</sub>) represents the NO<sub>x</sub> oxidation products. The (ΔNO<sub>z</sub>/ΔCO<sub>2</sub>)/E<sub>NO<sub>x</sub>-CO<sub>2</sub></sub> values represent the fraction of NO<sub>z</sub> produced per NO<sub>x</sub> emitted (i.e., NO<sub>z</sub> yield). The NO<sub>z</sub> yield would eventually approach 100% if there were no removal of NO<sub>z</sub>. However, it exhibited a broad maximum (10–15%) at plume ages of 2–3 days and then decreased with air mass aging after 3 days. Although this tendency does not represent a Lagrangian history for a particular event as mentioned earlier, it may be interpreted as follows. The NO<sub>z</sub> yield showed a net increase at plume ages of <2 days because the oxidation rate of NO<sub>x</sub> was faster than the removal rate of NO<sub>z</sub>. After 3 days when the NO<sub>x</sub>/NO<sub>y</sub> ratio decreased to as low as 10%, the oxidation of NO<sub>x</sub> was not an effective source of NO<sub>z</sub> any more, and the NO<sub>z</sub> yield showed a net decrease with air mass aging.

### 5.3.1. Interpretation of NO<sub>x</sub> Lifetime

[35] Here we investigate whether the estimated NO<sub>x</sub> loss rates in the plumes can be explained by the conversion of

NO<sub>x</sub> to HNO<sub>3</sub>. Detailed investigation is, however, somewhat speculative because of the lack of in situ measurements of NO<sub>x</sub> reservoirs such as HNO<sub>3</sub>, nitrate, and PAN during PEACE-A. It has been well documented that PAN can be an efficient reservoir of NO<sub>x</sub>. Near source regions, formation of PAN may be a net sink of NO<sub>x</sub>. As air masses age, thermal decomposition of PAN can become a net source of NO<sub>x</sub>. The role of PAN depends on whether its concentration level is above or below the equilibrium point. Thus the effects of PAN formation/destruction on NO<sub>x</sub> lifetime cannot be assessed in a meaningful way in the absence of PAN observations.

[36] NO<sub>x</sub> is oxidized to HNO<sub>3</sub> by reaction of NO<sub>2</sub> with OH during the daytime,



During the nighttime, NO<sub>3</sub> formation followed by hydrolysis of N<sub>2</sub>O<sub>5</sub> on sulfate aerosols could be important for the formation of HNO<sub>3</sub>.



First, the possible contribution from reaction (R1) is considered. For PEACE-A conditions, the photochemical lifetime of NO<sub>x</sub> against reaction (R1),  $\overline{\tau_{\text{NO}_x}}_{\text{OH}}$ , is estimated to be 2.5 ± 0.5 days. The diurnally averaged OH concentration (5 × 10<sup>5</sup> cm<sup>−3</sup>), the model-predicted NO<sub>2</sub>/NO<sub>x</sub> ratio (0.7–1.0), and the kinetic parameters recommended by Sander *et al.* [2000] were used for the calculation. The variability range of the OH concentration (see section 4.2) was not taken into consideration for the error estimate. Considering the estimated NO<sub>x</sub> lifetime of ~1.2 days, reaction (R1) accounts for about half of the NO<sub>x</sub> loss rate in the plumes, which suggests that processes other than the reaction of NO<sub>2</sub> + OH were also important for determining the NO<sub>x</sub> lifetime during PEACE-A. It should be noted that  $\overline{\tau_{\text{NO}_x}}$  is inversely proportional to the assumed OH concentration as is  $\overline{\tau_{\text{NO}_x}}_{\text{OH}}$  because it is proportional to  $\overline{\tau_{\text{C}_2\text{H}_4}}$  (equations (6) and (7)). Therefore the above result

### Japan-2 (F02L14) and Japan-4 (F03L08) plumes January 7 and 10, 2002

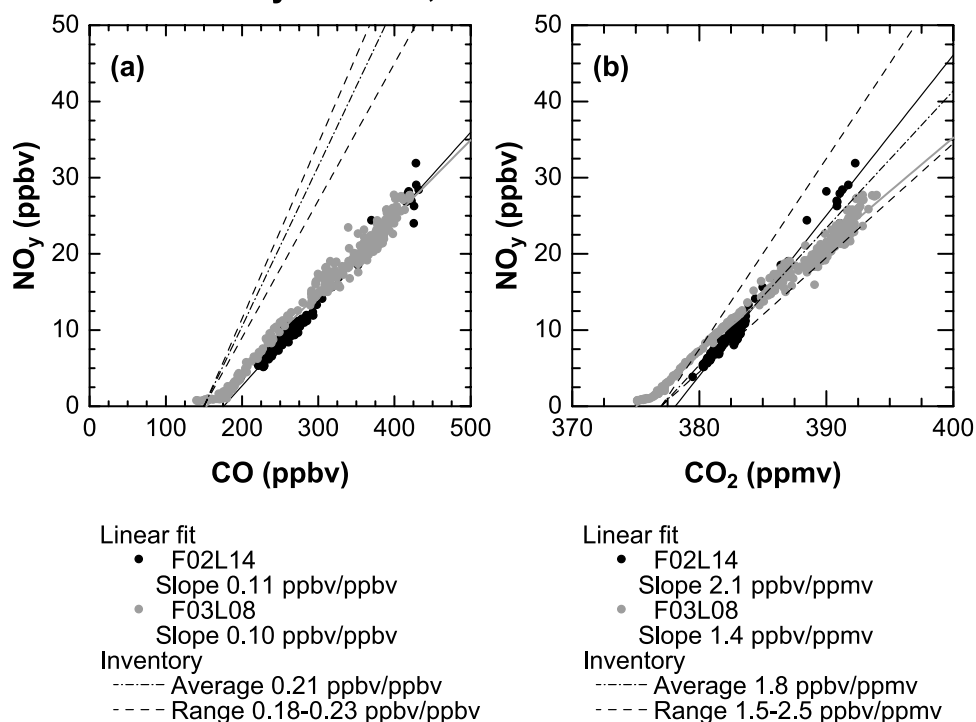


**Figure 10.** Correlations of (a) NO<sub>y</sub> with CO and (b) NO<sub>y</sub> with CO<sub>2</sub> observed below 1.6 km over Nagoya, Japan. Solid circles and shaded circles represent the Japan-2 (F02L14) and the Japan-4 (F03L08) plumes, respectively. Solid and shaded lines represent the regression lines. Emission ratios estimated from the emission inventory (dot-dashed line, average; dashed lines, maximum and minimum) are also shown.

(i.e.,  $\overline{\tau_{\text{NO}_x}}/\overline{\tau_{\text{NO}_2+\text{OH}}} \sim 0.5$ ) does not explicitly depend on the uncertainty in the assumed OH concentration.

[37] Second, possible contribution from reactions (R2)–(R4) is considered using the same box model as described in section 2.1. Aerosol chemical composition was not measured during PEACE-A. Here we assume that aerosol surface area ( $A$ ) measured by the Multiple-Angle Aerosol Spectrometer Probe (MASP) [Liley *et al.*, 2002] represents the surface area of sulfate aerosols. The surface area in the plumes ranged from 30 to 100  $\mu\text{m}^2/\text{cm}^3$  (median of 65  $\mu\text{m}^2/\text{cm}^3$ ) under cloud-free conditions. Earlier studies showed that the uptake coefficient ( $\gamma$ ) for reaction (R4) exhibits large variability, ranging from 0.01 to 0.1 (central value of 0.04) [Tie *et al.*, 2003, and references therein]. Using the above numbers as input parameters for the box model, the diurnally averaged NO<sub>x</sub> lifetime due to reactions (R2)–(R4) was estimated to be  $\sim 1$  day for the upper limit case ( $A = 100 \mu\text{m}^2/\text{cm}^3$ ,  $\gamma = 0.1$ ),  $\sim 4$  days for the middle case ( $A = 65 \mu\text{m}^2/\text{cm}^3$ ,  $\gamma = 0.04$ ), and  $\sim 30$  days for the lower limit case ( $A = 30 \mu\text{m}^2/\text{cm}^3$ ,  $\gamma = 0.01$ ). These estimates are subject to large uncertainties because of the wide range of  $\gamma$  and the assumption of the sulfate surface area. On the other hand, if we assume that the conditions in the plumes were between the upper limit and middle case, the NO<sub>x</sub> loss rate by reactions (R2)–(R4) would be comparable to reaction (R1). Therefore the NO<sub>x</sub> oxidation via reactions (R1)–(R4) can potentially explain most of the NO<sub>x</sub> loss processes in the plumes.

[38] Tie *et al.* [2003] examined the effect of reactions (R2)–(R4) on the NO<sub>x</sub> budget, on the basis of a global CTM and the aircraft measurement data obtained during the Tropospheric Ozone Production about the Spring Equinox (TOPSE) mission. They found that this heterogeneous process plays an important role in controlling NO<sub>x</sub> concentrations in the Northern Hemispheric middle-to-high latitudes in wintertime. According to their simulations, the NO<sub>x</sub> loss rate against reaction (R2), which was the rate-limiting step for reactions (R2)–(R4), was comparable to or even faster than the one against reaction (R1) under similar conditions (altitudes  $< 3$  km, latitudes  $25^\circ$ – $40^\circ\text{N}$ , December). Thus the findings of Tie *et al.* [2003] strongly support the hypothesis in this study.

#### 5.3.2. Interpretation of NO<sub>y</sub> Lifetime

[39] As mentioned earlier, it was found that only 10–20% of the NO<sub>y</sub> compounds emitted from surface sources in east Asia remained in the plumes after 4 days. This fraction is smaller than the NO<sub>y</sub> export efficiencies of 20–40% in the boundary layer over the western Pacific during TRACE-P [Koike *et al.*, 2003; Miyazaki *et al.*, 2003], although the relationship between the export efficiencies and air mass aging was not discussed in those studies. Stohl *et al.* [2002] estimated an effective mean NO<sub>y</sub> lifetime of 1.7–1.8 days in air masses exported from the United States to the North Atlantic (mainly at  $35^\circ$ – $50^\circ\text{N}$ ), on the basis of aircraft data obtained during the North Atlantic Regional Experiment in spring 1996 and fall 1997

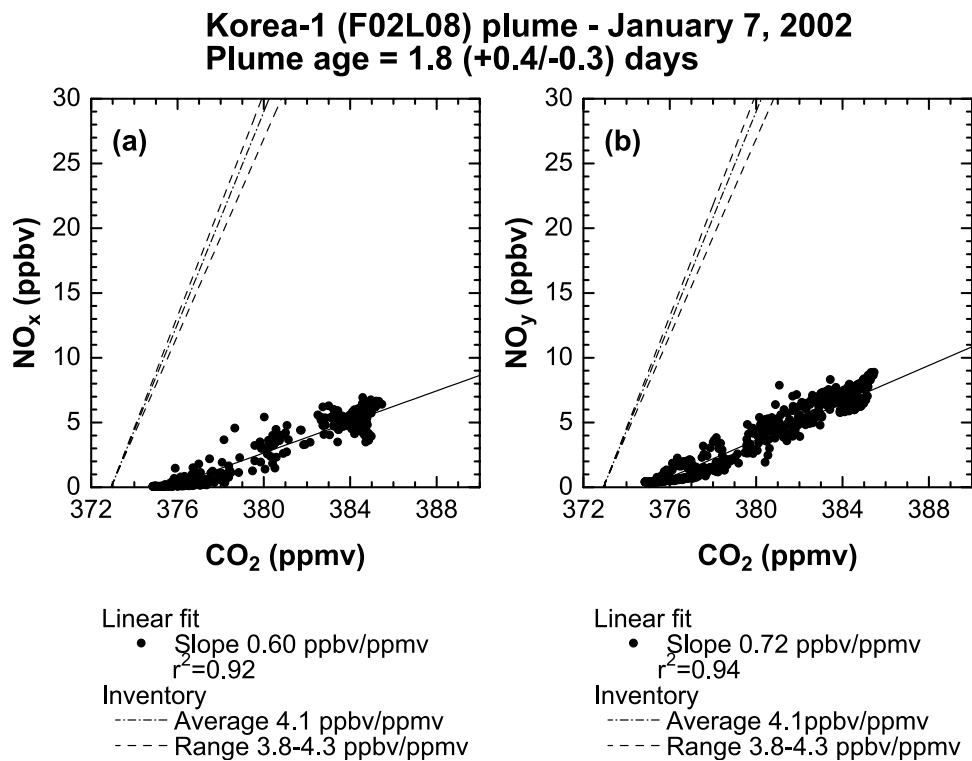


**Figure 11.** Correlations of (a)  $\text{NO}_x$  and (b)  $\text{NO}_y$  with  $\text{CO}_2$  in the Korea-1 (F02L08) plume (same plume as used in Figure 6). Solid lines are linear regression lines. The dot-dashed line and two dashed lines represent the average, maximum, and minimum values of the  $\text{NO}_x/\text{CO}_2$  emission ratio from the Korea region, respectively.

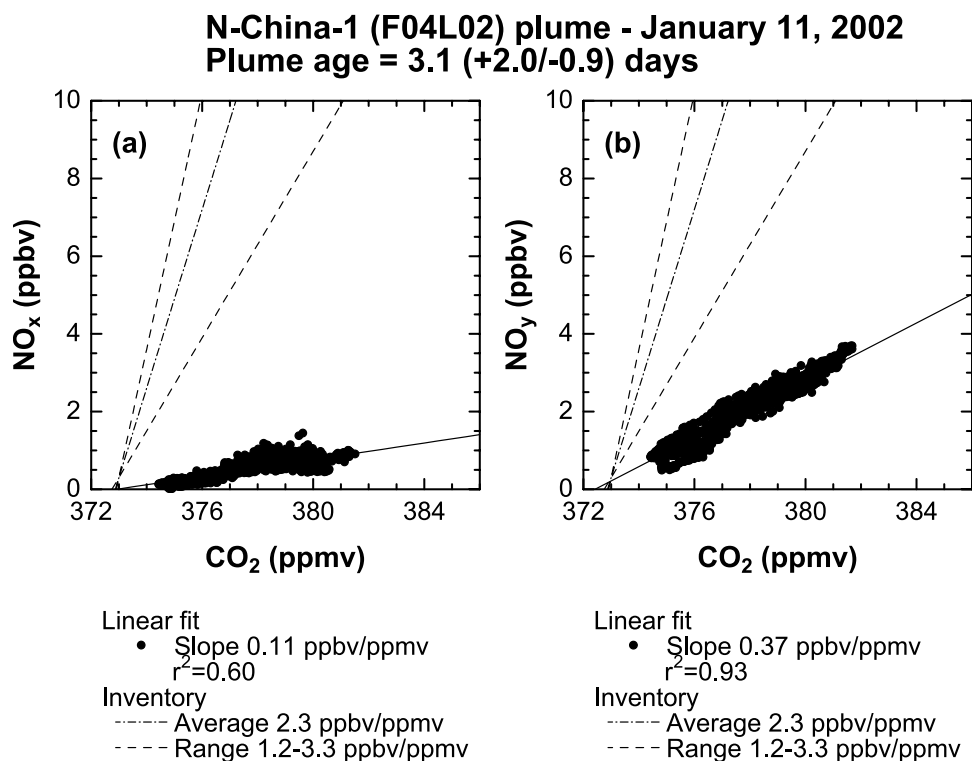


**Figure 12.** Same plot as Figure 11 but for the N-China-1 (F04L02) plume (same plume as used in Figure 7).

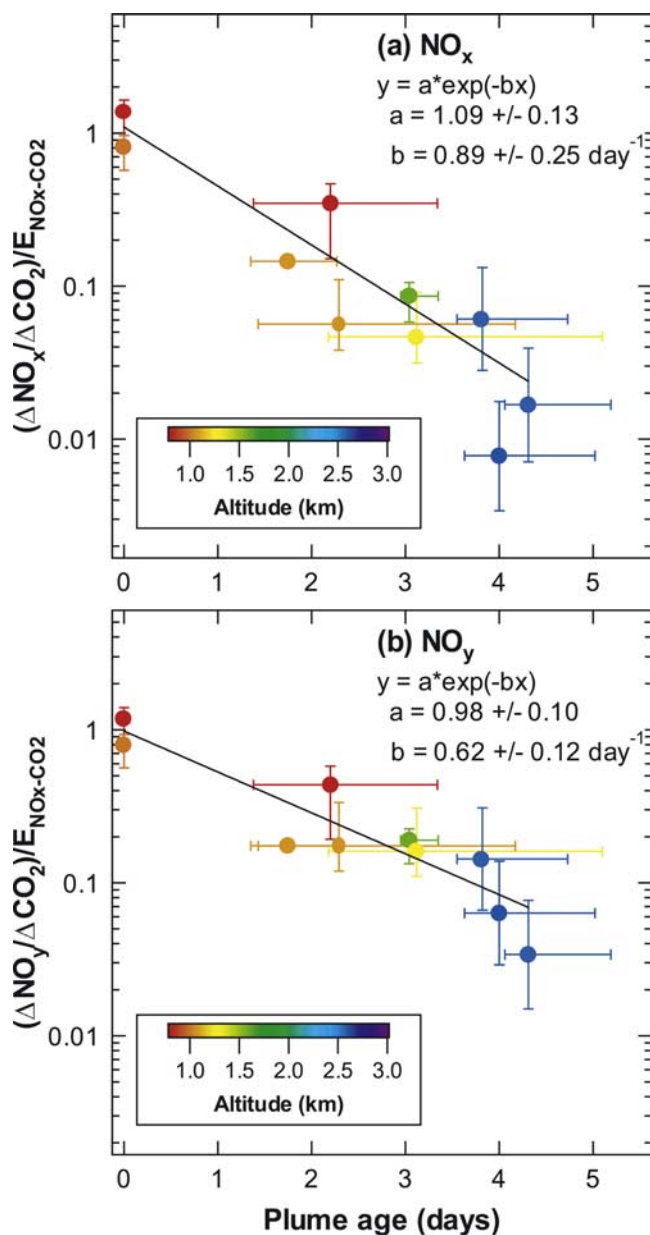


**Figure 13.** (a)  $(\Delta\text{NO}_x/\Delta\text{CO}_2)/E_{\text{NO}_x\text{-CO}_2}$  and (b)  $(\Delta\text{NO}_y/\Delta\text{CO}_2)/E_{\text{NO}_x\text{-CO}_2}$  as a function of plume age defined by equation (6). Data points are colored on the basis of average sampling altitudes. Solid curves were determined by a least squares fit to the data. The error bars were determined from fitting errors for the NO<sub>x</sub>-CO<sub>2</sub> (or NO<sub>y</sub>-CO<sub>2</sub>) correlations and the maximum and minimum values of the NO<sub>x</sub> to CO<sub>2</sub> emission ratios.

(NARE 96, 97). The NO<sub>y</sub> lifetime estimated in this study ( $1.7 \pm 0.5$ ) is close to the one estimated by Stohl et al. It is important to note that both this study and that of Stohl et al. estimated NO<sub>y</sub> lifetimes of 1–2 days, despite the significant differences in the type of emission sources and meteorological conditions. A common feature found in these two experiments is that a large fraction of NO<sub>y</sub> compounds emitted from surface sources were removed within 1–2 days. The transport time of 1–2 days roughly

corresponds to the horizontal travel distance of 1000–2000 km in the boundary layer under PEACE-A conditions. Therefore this finding suggests that the processing near the source regions is critical in determining the NO<sub>y</sub> abundance.

## 6. Summary and Conclusions

[40] Removal of NO<sub>x</sub> and NO<sub>y</sub> in Asian outflow plumes below 4 km was investigated using aircraft data obtained during the PEACE-A campaign conducted over the western Pacific in January 2002. Correlations of CO with CO<sub>2</sub> and back trajectories were used to identify the plumes transported from source regions in the Asian continent. The plumes originating from Japan (Nagoya) or Korea (Pusan) exhibited relatively low  $\Delta\text{CO}/\Delta\text{CO}_2$  ratios (14–24 ppbv/ppmv), while those from China showed high  $\Delta\text{CO}/\Delta\text{CO}_2$  ratios (28–48 ppbv/ppmv). The observed  $\Delta\text{CO}/\Delta\text{CO}_2$  ratios generally fall within the variability range of the CO/CO<sub>2</sub> emission ratios estimated from the trajectories and the emission inventory on the basis of the work of *Streets et al.* [2003], demonstrating the overall consistency among the aircraft measurements and the emission characterization. The present analysis indicates that  $\Delta\text{CO}/\Delta\text{CO}_2$  ratios can

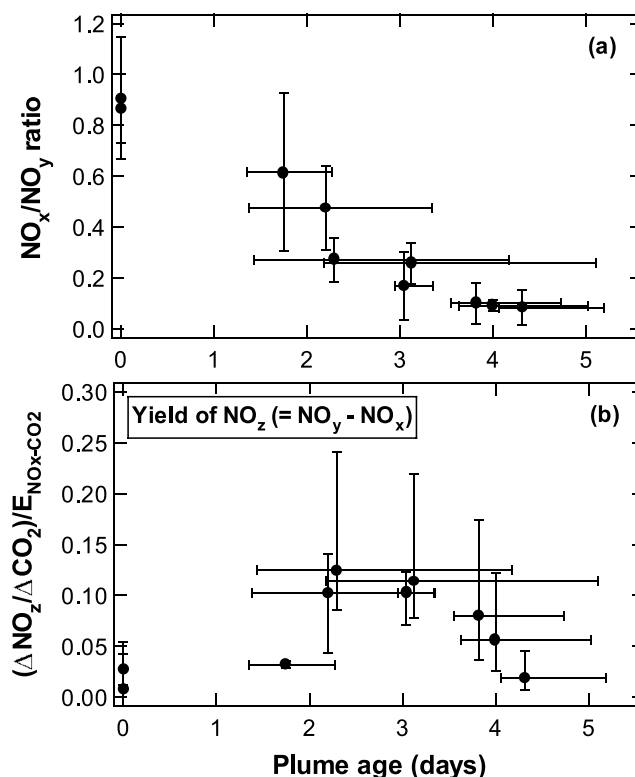


**Figure 14.** (a) Average NO<sub>x</sub>/NO<sub>y</sub> ratio and (b)  $(\Delta\text{NO}_z/\Delta\text{CO}_2)/E_{\text{NO}_x\text{-CO}_2}$  as a function of plume age, where NO<sub>z</sub>(=NO<sub>y</sub> – NO<sub>x</sub>) represents the NO<sub>x</sub> oxidation products. The error bars for the NO<sub>x</sub>/NO<sub>y</sub> ratios represent 1-σ of the average. The error bars for the  $(\Delta\text{NO}_z/\Delta\text{CO}_2)/E_{\text{NO}_x\text{-CO}_2}$  were determined from fitting errors for the NO<sub>z</sub>-CO<sub>2</sub> correlations and the maximum and minimum values of the NO<sub>x</sub> to CO<sub>2</sub> emission ratios.

be used as a good tracer for investigating the origins of anthropogenic plumes when the enhancements of CO and CO<sub>2</sub> are large enough and the correlation is tight.

[41] The photochemical age of the plumes was estimated using the observed  $\Delta\text{C}_2\text{H}_4/\Delta\text{C}_2\text{H}_2$  ratios and the OH concentration calculated by a constrained photochemical box model. Removal of NO<sub>x</sub> was investigated using  $\Delta\text{NO}_x/\Delta\text{CO}_2$  ratios and plume age. The photochemical lifetime of NO<sub>x</sub> was estimated to be  $1.2 \pm 0.4$  days, which was  $\sim 2$  times shorter than the lifetime against reaction of NO<sub>2</sub> + OH. This result suggests that other processes were also important in determining the NO<sub>x</sub> lifetime during the PEACE-A period. It is likely that NO<sub>x</sub> oxidation to NO<sub>3</sub> followed by N<sub>2</sub>O<sub>5</sub> formation and hydrolysis was another important factor controlling the NO<sub>x</sub> lifetime under PEACE-A conditions.

[42] The lifetime of NO<sub>y</sub> estimated using  $\Delta\text{NO}_y/\Delta\text{CO}_2$  and plume age was found to be  $1.7 \pm 0.5$  days, indicating the rapid removal of NO<sub>x</sub> oxidation products (NO<sub>z</sub> = NO<sub>y</sub> - NO<sub>x</sub>) in the plumes. The maximum NO<sub>z</sub> yield (i.e., fraction of NO<sub>z</sub> produced per NO<sub>x</sub> emitted) during the transport was only 10–15%. This maximum appeared at plume ages of 2–3 days, when the NO<sub>x</sub> oxidation and NO<sub>z</sub> removal rates were likely balanced. The NO<sub>y</sub> lifetime obtained in this study was comparable to the NO<sub>y</sub> lifetime of 1.7–1.8 days that has previously been reported for outflow from the United States, although there are significant differences in the types of emission sources and meteorological conditions between these two studies. A common feature found in these experiments is that a large fraction of NO<sub>y</sub> compounds emitted from surface sources was removed within 1–2 days. This finding suggests the importance of chemical/physical processing (i.e., NO<sub>x</sub> oxidation and dry/wet deposition of NO<sub>y</sub>) near the source regions in determining the NO<sub>y</sub> abundance on a regional or even global scale.

[43] **Acknowledgments.** The authors thank the staff of Diamond Air Service (DAS) for their support and efforts during the aircraft measurements. The PEACE-A mission was partially funded by the Japanese Ministry of Education, Culture, Sports, Science and Technology (MEXT). The ITCT 2K2/PEACE campaigns were conducted under the framework of the International Global Atmospheric Chemistry (IGAC) project (<http://www.igac.noaa.gov/>).

## References

- Andreae, M. O., B. E. Anderson, D. R. Blake, J. D. Bradshaw, J. E. Collins, G. L. Gregory, G. W. Sachse, and M. C. Shipham (1994), Influence of plumes from biomass burning on atmospheric chemistry over the equatorial and tropical South Atlantic during CITE 3, *J. Geophys. Res.*, *99*, 12,793–12,808.
- Atkinson, R., D. L. Baulch, R. A. Cox, R. F. Hampson Jr., J. A. Kerr, and J. Troe (1992), Evaluated kinetic and photochemical data for atmospheric chemistry: Supplement IV, *J. Phys. Chem. Ref. Data*, *21*(6), 1125–1568.
- Blake, N., et al. (2003), NMHCs and halocarbons in Asian continental outflow during the Transport and Chemical Evolution over the Pacific (TRACE-P) field campaign: Comparison with PEM-West B, *J. Geophys. Res.*, *108*(D20), 8806, doi:10.1029/2002JD003367.
- Calvert, J. G., R. Atkinson, J. A. Kerr, S. Madronich, G. K. Moortgat, T. J. Wallington, and G. Yarwood (2000), *The Mechanism of Atmospheric Oxidation of the Alkenes*, Oxford Univ. Press, New York.
- Hinds, W. C. (1998), *Aerosol Technology*, John Wiley, Hoboken, N. J.
- Hobbs, P. V., P. Sinha, R. J. Yokelson, T. J. Christian, D. R. Blake, S. Gao, T. W. Kirchstetter, T. Novakov, and P. Pilewskie (2003), Evolution of gases and particles from a savanna fire in South Africa, *J. Geophys. Res.*, *108*(D13), 8485, doi:10.1029/2002JD002352.
- Hoell, J. M., D. D. Davis, S. C. Liu, R. Newell, M. Shipham, H. Akimoto, R. J. McNeal, R. J. Bendura, and J. W. Drewry (1996), Pacific Exploratory Mission-West A (PEM-West A): September–October 1991, *J. Geophys. Res.*, *101*, 1641–1653.
- Hoell, J. M., D. D. Davis, S. C. Liu, R. E. Newell, H. Akimoto, R. J. McNeal, and R. J. Bendura (1997), The Pacific Exploratory Mission-West Phase B: February–March, 1994, *J. Geophys. Res.*, *102*, 28,223–28,239.
- Irie, H., Y. Kondo, M. Koike, N. Takegawa, A. Tabazadeh, J. M. Reeves, G. W. Sachse, S. A. Vay, B. E. Anderson, and M. J. Mahoney (2004), Liquid ternary aerosols of HNO<sub>3</sub>/H<sub>2</sub>SO<sub>4</sub>/H<sub>2</sub>O in the Arctic tropopause region, *Geophys. Res. Lett.*, *31*, L01105, doi:10.1029/2003GL018678.
- Jacob, D. J., J. H. Crawford, M. M. Kleb, V. S. Connors, R. J. Bendura, J. L. Raper, G. W. Sachse, J. C. Gille, L. Emmons, and C. L. Heald (2003), Transport and Chemical Evolution over the Pacific (TRACE-P) aircraft mission: Design, execution, and first results, *J. Geophys. Res.*, *108*(D20), 9000, doi:10.1029/2002JD003276.
- Jaffe, D., H. Price, D. Parrish, A. Goldstein, and J. Harris (2003), Increasing background ozone during spring on the west coast of North America, *Geophys. Res. Lett.*, *30*(12), 1613, doi:10.1029/2003GL017024.
- Kita, K., et al. (2002), Photochemical production of ozone in the upper troposphere in association with cumulus convection over Indonesia, *J. Geophys. Res.*, *107*, 8400, doi:10.1029/2001JD000844. [printed 108(D3), 2003]
- Koike, M., et al. (2003), Export of anthropogenic reactive nitrogen and sulfur compounds from the east Asia region in spring, *J. Geophys. Res.*, *108*(D20), 8789, doi:10.1029/2002JD003284.
- Kondo, Y., et al. (1997a), Profiles and partitioning of reactive nitrogen over the Pacific Ocean in winter and early spring, *J. Geophys. Res.*, *102*, 28,405–28,424.
- Kondo, Y., S. Kawakami, M. Koike, D. W. Fahey, H. Nakajima, Y. Zhao, N. Toriyama, M. Kanada, G. W. Sachse, and G. L. Gregory (1997b), The performance of an aircraft instrument for the measurement of NO<sub>y</sub>, *J. Geophys. Res.*, *102*, 28,663–28,671.
- Kondo, Y., M. Ko, M. Koike, S. Kawakami, and T. Ogawa (2002), Preface to special section on Biomass Burning and Lightning Experiment (BIBLE), *J. Geophys. Res.*, *107*, 8397, doi:10.1029/2002JD002401. [printed 108(D3), 2003]
- Kondo, Y., et al. (2003), Uptake of reactive nitrogen on cirrus cloud particles in the upper troposphere and lowermost stratosphere, *Geophys. Res. Lett.*, *30*(4), 1154, doi:10.1029/2002GL016539.
- Kondo, Y., et al. (2004a), Impacts of biomass burning in Southeast Asia on ozone and reactive nitrogen over the western Pacific in spring, *J. Geophys. Res.*, *109*, D15S12, doi:10.1029/2003JD004203.
- Kondo, Y., et al. (2004b), Photochemistry of ozone over the western Pacific from winter to spring, *J. Geophys. Res.*, *109*, D23S02, doi:10.1029/2004JD004871, in press.
- Liley, J. B., et al. (2002), Black carbon in aerosol during BIBLE-B, *J. Geophys. Res.*, *107*, 8399, doi:10.1029/2001JD000845. [printed 108(D3), 2003]
- Machida, T., K. Kita, Y. Kondo, D. Blake, S. Kawakami, G. Inoue, and T. Ogawa (2002), Vertical and meridional distributions of the atmospheric CO<sub>2</sub> mixing ratio between northern midlatitudes and southern subtropics, *J. Geophys. Res.*, *107*, 8401, doi:10.1029/2001JD000910. [printed 108(D3), 2003]
- McKeen, S. A., S. C. Liu, E.-Y. Hsie, X. Lin, J. D. Bradshaw, S. Smyth, G. L. Gregory, and D. R. Blake (1996), Hydrocarbon ratios during PEM-WEST A: A model perspective, *J. Geophys. Res.*, *101*, 2087–2109.
- Miyazaki, Y., et al. (2003), Synoptic-scale transport of reactive nitrogen over the western Pacific in spring, *J. Geophys. Res.*, *108*(D20), 8788, doi:10.1029/2002JD003248.
- Nicks, D. K., Jr., et al. (2003), Fossil-fueled power plants as a source of atmospheric carbon monoxide, *J. Environ. Monit.*, *5*, 35–39.
- Oshima, N., et al. (2004), Asian chemical outflow to the Pacific in late spring observed during the PEACE-B aircraft campaign, *J. Geophys. Res.*, *109*, D23S05, doi:10.1029/2004JD004976, in press.
- Palmer, P. I., D. J. Jacob, D. B. A. Jones, C. L. Heald, R. M. Yantosca, J. A. Logan, G. W. Sachse, and D. G. Streets (2003), Inverting for emissions of carbon monoxide from Asia using aircraft observations over the western Pacific, *J. Geophys. Res.*, *108*(D21), 8828, doi:10.1029/2003JD003397.
- Parrish, D. D., C. J. Hahn, E. J. Williams, R. B. Norton, and F. C. Fehsenfeld (1992), Indications of photochemical histories of Pacific air masses from measurements of atmospheric trace species at Point Arena, California, *J. Geophys. Res.*, *97*, 15,883–15,901.
- Sander, S. P., et al. (2000), Chemical kinetics and photochemical data for use in stratospheric modeling, Evaluation number 13, *JPL Publ.*, 00-03.
- Shirai, T., et al. (2003), Emission estimates of selected volatile organic compounds from tropical savanna burning in northern Australia, *J. Geophys. Res.*, *108*(D3), 8406, doi:10.1029/2001JD000841.

- Song, C. H., G. Chen, S. R. Hanna, J. Crawford, and D. D. Davis (2003), Dispersion and chemical evolution of ship plumes in the marine boundary layer: Investigation of O<sub>3</sub>/NO<sub>y</sub>/HO<sub>x</sub> chemistry, *J. Geophys. Res.*, *108*(D4), 4143, doi:10.1029/2002JD002216.
- Stohl, A., M. Trainer, T. B. Ryerson, J. S. Holloway, and D. D. Parrish (2002), Export of NO<sub>y</sub> from the North American boundary layer during 1996 and 1997 North Atlantic Regional Experiments, *J. Geophys. Res.*, *107*(D11), 4131, doi:10.1029/2001JD000519.
- Streets, D. G., et al. (2003), An inventory of gaseous and primary aerosol emissions in Asia in the year 2000, *J. Geophys. Res.*, *108*(D21), 8809, doi:10.1029/2002JD003093.
- Takegawa, N., et al. (2001), Airborne vacuum ultraviolet resonance fluorescence instrument for in situ measurement of CO, *J. Geophys. Res.*, *106*, 24,237–24,244.
- Takegawa, N., et al. (2003), Removal of NO<sub>x</sub> and NO<sub>y</sub> in biomass burning plumes in the boundary layer over northern Australia, *J. Geophys. Res.*, *108*(D10), 4308, doi:10.1029/2002JD002505.
- Tie, X., et al. (2003), Effect of sulfate aerosol on tropospheric NO<sub>x</sub> and ozone budgets: Model simulations and TOPSE evidence, *J. Geophys. Res.*, *108*(D4), 8364, doi:10.1029/2001JD001508.
- Vay, S. A., et al. (2003), Influence of regional-scale anthropogenic emissions on CO<sub>2</sub> distributions over the western North Pacific, *J. Geophys. Res.*, *108*(D20), 8801, doi:10.1029/2002JD003094.
- Woo, J.-H., et al. (2003), Contribution of biomass and biofuel emissions to trace gas distributions in Asia during the TRACE-P experiment, *J. Geophys. Res.*, *108*(D21), 8812, doi:10.1029/2002JD003200.
- Yokelson, R. J., I. T. Bertschi, T. J. Christian, P. V. Hobbs, D. E. Ward, and W. M. Hao (2003), Trace gas measurements in nascent, aged, and cloud-processed smoke from African savanna fires by airborne Fourier transform infrared spectroscopy (AFTIR), *J. Geophys. Res.*, *108*(D13), 8478, doi:10.1029/2002JD002322.
- Zhang, J., K. R. Smith, Y. Ma, S. Ye, F. Jiang, W. Qi, P. Liu, M. A. K. Khalil, R. A. Rasmussen, and S. A. Thorneloe (2000), Greenhouse gases and other airborne pollutants from household stoves in China: A database for emission factors, *Atmos. Environ.*, *34*, 4537–4549.
- D. R. Blake, Department of Chemistry, University of California, Irvine, Irvine, CA 92697-2025, USA. (dblake@uci.edu)
- G. R. Carmichael and J.-H. Woo, Center for Global and Regional Environmental Research, University of Iowa, Iowa, IA 52242, USA. (gcarmich@engineering.uiowa.edu; woojh21@cgrrer.uiowa.edu)
- G. Chen, NASA Langley Research Center, Hampton, VA 23681-0001, USA. (g.chen@larc.nasa.gov)
- K. Kita, Department of Environmental Sciences, Faculty of Science, Ibaraki University, 2-1-1 Bunkyo, Mito, Ibaraki 310-8512, Japan. (kita@env.sci.ibaraki.ac.jp)
- M. Koike, Department of Earth and Planetary Science, Graduate School of Science, University of Tokyo, 7-3-1 Hongo, Bunkyo-ku, Tokyo 113-0033, Japan. (koike@eps.s.u-tokyo.ac.jp)
- Y. Kondo, Y. Miyazaki, and N. Takegawa, Research Center for Advanced Science and Technology, University of Tokyo, 4-6-1 Komaba, Tokyo 153-8904, Japan. (kondo@atmos.rcast.u-tokyo.ac.jp; yuzom@atmos.rcast.u-tokyo.ac.jp; takegawa@atmos.rcast.u-tokyo.ac.jp)
- J. B. Liley, National Institute of Water and Atmospheric Research, Private Bag 50061, Omakau, Central Otago, New Zealand. (b.liley@niwa.co.nz)
- T. Machida and T. Shirai, National Institute for Environmental Studies, Tsukuba 305-0053, Japan. (tmachida@nies.go.jp; shirai@eorc.jaxa.jp)
- T. Ogawa, Earth Observation Research and Application Center, Japan Aerospace Exploration Agency, 1-8-10 Harumi, Tokyo 104-6023, Japan. (ogawa.toshihiro@jaxa.jp)
- D. G. Streets, Decision and Information Sciences Division, Argonne National Laboratory, Argonne, IL 60439, USA. (dstreets@anl.gov)
- T. Watai, Global Environmental Forum, Tsukuba 305-0053, Japan. (watai.tomonori@nies.go.jp)